Chapter 4

Analysis of Interdigital Transducers

As noted in Chapter 1, interdigital transducers are used in all practical surface-wave devices, and in many devices the performance of the transducers is the main factor determining the device performance. A detailed understanding of the behaviour of transducers is therefore crucial for both analysis and design of the devices. This chapter describes methods for transducer analysis, and for analysis of devices comprising two transducers. Most of the analysis is based on the Green's function derived in Chapter 3, using an approximation called the "quasi-static approximation" for simplicity.

Section 4.1 describes the delta-function model, which gives a straightforward approximate analysis. Despite being over-simplified, this model is very convenient to use, and illustrates some important features directly. It is particularly useful for transducer design, as will be considered in later chapters. Section 4.2 discusses some important second-order effects that are neglected in the delta-function model, and also gives a comparative discussion of several other methods for transducer analysis.

The quasi-static approximation is introduced in Section 4.3, which derives results applicable to both transducers and multi-strip couplers, and the main properties of transducers are then derived in Section 4.4. The remaining sections are concerned with some applications of this basic analysis. In Sections 4.5 and 4.6 some particular restrictions are imposed on the transducer geometry; these restrictions enable some useful results, applicable to most interdigital devices, to be derived. Finally, Sections 4.7 and 4.8 are concerned with analysis of devices comprising two transducers.

4.1. DELTA-FUNCTION MODEL

This model was introduced by Tancrell and Holland [79, 80], and a closely related approach called the "impulse model" was described later by Hartmann *et al.* [81].

(a) Launching Transducer. We first consider generation of surface waves by a uniform transducer, as shown in Figure 4.1(a). The transducer electrodes are all identical, and are connected alternately to the two bus-bars. When a voltage is applied

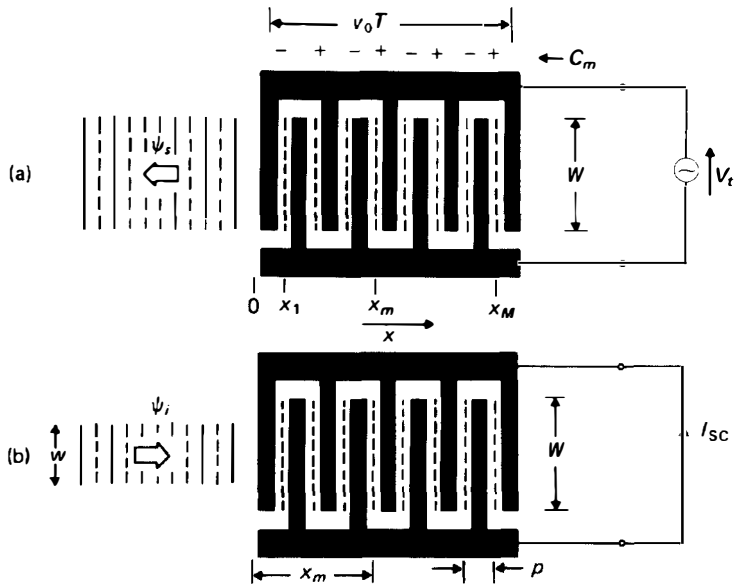

FIGURE 4.1. Uniform transducer: launching and reception.

an electric field is set up in each inter-electrode gap, and surface waves are generated. It is assumed that each gap can be regarded as an independent source, launching surface waves with amplitudes proportional to the voltage difference between the adjacent electrodes. We also assume that an adequate approximation is obtained by taking each source to be strongly localised, so that the sources can be represented by the broken lines in Figure 4.1(a), midway between the electrodes. We consider waves generated to the left, though the transducer will also generate waves to the right.

The wave amplitude is denoted by $\psi_s(x)$, and this will be proportional to the potential $\phi_s(x)$ associated with the wave. A precise physical definition for $\psi_s(x)$ is not needed in this model, though its relation to the surface wave power flow is given later. For the source located at x_m, the wave generated to the left, at frequency ω, is written as

$$\psi_s(x) = EV_iC_m \exp [jk_0(x - x_m)], \tag{4.1}$$

where a factor $\exp(j\omega t)$ is implicit and the real part is to be taken. Here the factor $C_m = \pm 1$ accounts for the alternating polarities of the fields in the gaps, as shown in Figure 4.1(a), and E is a constant. The wavenumber k_0 is taken to be ω/v_0, where v_0 is the free-surface velocity. Equation (4.1) thus assumes that each source generates waves which propagate out of the transducer, unaffected by the electrodes that they pass under. In fact, the electrodes reflect the waves to some extent, and they also perturb the surface-wave velocity. It is assumed that these effects can be neglected, as is often found to be the case, particularly when the piezoelectric coupling of the material is weak.

The material can be taken to be linear, so that the total amplitude of the wave generated by the transducer is the sum of the contributions due to individual sources.

Thus the total wave amplitude is

$$\psi_s(x) = V_t E A(\omega) \exp(jk_0 x), \tag{4.2}$$

where

$$A(\omega) = \sum_{m=1}^{M} C_m \exp(-jk_0 x_m) \tag{4.3}$$

and M is the number of sources. The product $EA(\omega)$ is essentially the *frequency response* of the transducer, giving the surface wave amplitude as a function of frequency. The function $A(\omega)$, determined by the relative positions and the polarities of the elements, is the *array factor*, and E is the *element factor*. A detailed analysis, given in later sections, shows that E varies a little with frequency. However, $A(\omega)$ is found to vary much more rapidly than E and, in the delta-function model, a reasonable approximation is obtained by taking E to be constant. Thus the frequency response is essentially given by the array factor alone, and since this is readily found from the transducer geometry the model is convenient to use. The element factor is evaluated in Section 4.5.3.

For the uniform transducer considered here, the summation in equation (4.3) can be written in a more convenient form. Since C_m alternates between $+1$ and -1 we may write $C_m = -C_1 \exp(jm\pi)$. Also, taking the spacing of the sources to be p, their locations may be written $x_m = mp$. With these substitutions, equation (4.3) is readily summed as a geometric progression. Since the phase is of little interest here, we consider the magnitude of the array factor, which is found to be

$$|A(\omega)| = \left|\frac{\sin M\theta/2}{\sin \theta/2}\right|, \tag{4.4}$$

where $\theta = k_0 p - \pi$. We also define ω_c as the frequency at which the transducer periodicity, $2p$, equals the surface-wave wavelength, so that $\omega_c = \pi v_0/p$. We then have

$$\theta = \pi(\omega - \omega_c)/\omega_c. \tag{4.5}$$

The magnitude of the array factor is shown, as a function of ω, in Figure 4.2. The first main peak occurs at frequency ω_c, and the response in this region is called the fundamental response. Harmonic responses of equal magnitude occur at odd multiples of ω_c.

The fundamental response is of most interest. If ω is near ω_c, θ is small and the magnitude of the array factor is, approximately,

$$|A(\omega)| \approx M \left|\frac{\quad}{\quad}\right|. \tag{4.6}$$

For this function, the zeros nearest to ω_c are at $\omega = \omega_c \pm 2\omega_c/M$. Roughly speaking, the transducer responds effectively over a band of frequencies bounded by the points $\omega = \omega_c \pm \omega_c/M$, where the amplitude is about 4 dB below its maximum value. Thus the bandwidth can be taken to be $\Delta\omega = 2\omega_c/M$. Now, the length of the transducer

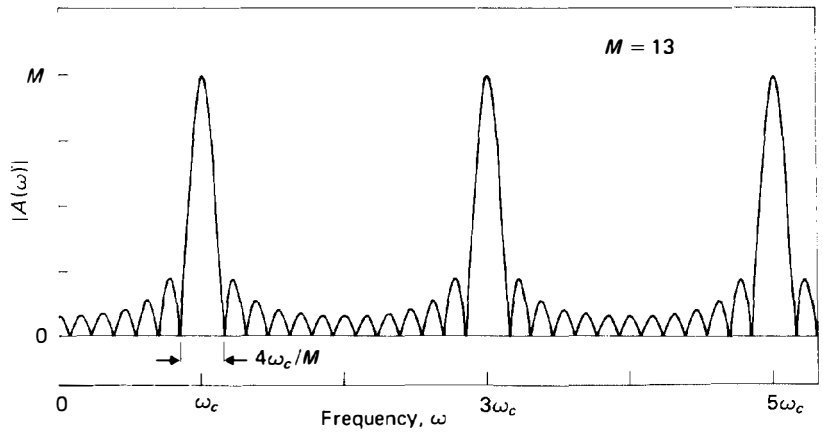

FIGURE 4.2. Magnitude of array factor for a uniform transducer.

is approximately Mp, which corresponds to a surface-wave propagation time $T = Mp/v_0$. Thus the bandwidth can be written as

$$\Delta\omega = 2\pi/T. \tag{4.7}$$

Thus the bandwidth, in Hz, is simply the reciprocal of the transducer length, measured in time units.

It was stated earlier that the element factor E in equation (4.2) can be taken to be independent of frequency. This is valid for the fundamental response, where ω is close to ω_c, and for a harmonic response, where ω is close to an odd multiple of ω_c. However, the element factor has a strong effect on the relative levels of the harmonics. In particular, it is shown in a later section that the third harmonic, centred at $\omega = 3\omega_c$, is absent altogether if the electrode widths are equal to $p/2$.

(b) Reception. We now consider the same transducer receiving a surface-wave beam, as shown on Figure 4.1(b). The transducer is taken to be shorted, and generates a current I_{sc}. The incident beam has a width, w, less than or equal to the transducer aperture, W. The amplitude of the incident beam is written as

$$\psi_i(x) = \psi_{i0} \exp(-jk_0 x), \tag{4.8}$$

where ψ_{i0} is a constant. As before, it is assumed that the surface wave is not perturbed by the presence of the electrodes, so that equation (4.8) gives the wave amplitude at all x.

For generation of surface waves, the transducer was regarded as an array of localised sources, shown by the broken lines in Figure 4.1(a). For a receiving transducer, each of these sources becomes a receiving element, making a contribution to the current I_{sc}. Clearly, the element at x_m contributes a current proportional to $C_m\psi_i(x_m)$. The total current is simply the sum of these contributions, with a proportionality constant Ew which is justified below. Thus,

$$I_{sc} = \psi_{i0} wE \sum_{m=1}^{M} C_m \exp(-jk_0 x_m), \quad \text{for } w \leqslant W. \tag{4.9}$$

Comparing with equation (4.3), we have $I_{sc} = \psi_{i0} wEA(\omega)$. Thus the frequency response, $EA(\omega)$, applies to the reception process as well as to the launching process, as expected by reciprocity.

In equation (4.9), I_{sc} is taken to be proportional to w, and this is justified by the following argument. Physically, the current arises because the surface wave induces charges on the electrodes. The charge density is proportional to the wave amplitude ψ_{i0}, and is uniform over the width of the beam. However, the current flowing out of any one electrode is given by the total charge on it, and must therefore be proportional to the beamwidth w. Hence the transducer current I_{sc} is also proportional to w.

The use of the coefficient E in equation (4.9) is justified by the observation that the magnitudes of the surface wave amplitudes, ψ_s and ψ_i, have not so far been specified. In equation (4.9) E is proportional to $1/\psi_{i0}$, while in equation (4.2) for the launching process E is proportional to the magnitude of $\psi_s(x)$. Thus, if a suitable definition is used for ψ_s and ψ_i, the same element factor, E, may be used in equations (4.2) and (4.9). This is assumed to be the case, and consequently the magnitudes of ψ_s and ψ_i are determined. It is found that, for the launching transducer, Figure 4.1(a), the power of the surface wave beam radiated to the left is given by

$$P_s = \tfrac{1}{4} W |\psi_s|^2, \tag{4.10}$$

where W is the beam width. A similar relation applies for the incident beam in Figure 4.1(b). This relation can be proved by considering the power conversion efficiency of the transducer, for launching and reception of surface waves, making use of equations (4.2) and (4.9). From the analysis in later sections of this chapter, it also follows that $\psi_s(x)$ is proportional to the potential $\phi_s(x)$ associated with the propagating wave. Comparing equation (4.10) with the power flow given by equation (3.34) shows that the magnitude of $\psi_s(x)$ is given by

$$|\psi_s(x)| = |\phi_s(x)|(\omega/\Gamma_s)^{1/2}, \tag{4.11}$$

where the constant Γ_s, given by equation (3.39), is a measure of the piezoelectric coupling of the substrate material.

(c) Apodised Transducers. To appreciate the behaviour of an apodised transducer, it is necessary to consider the response of a surface-wave device having two transducers. Here, the device of Figure 4.3 is considered, where transducer A is apodised and transducer B is unapodised. To preserve the symmetry, the source locations in the two transducers are referred to different axes, x for transducer A and x' for transducer B; in each transducer, the axis is directed away from the other transducer. A voltage V_t, with frequency ω, is applied to transducer A. Transducer B is shorted, and produces a current I_{sc}.

In transducer A, the sources are taken to exist only where electrodes of differing polarity overlap. The length of source m will be denoted a_m, and it is assumed that the

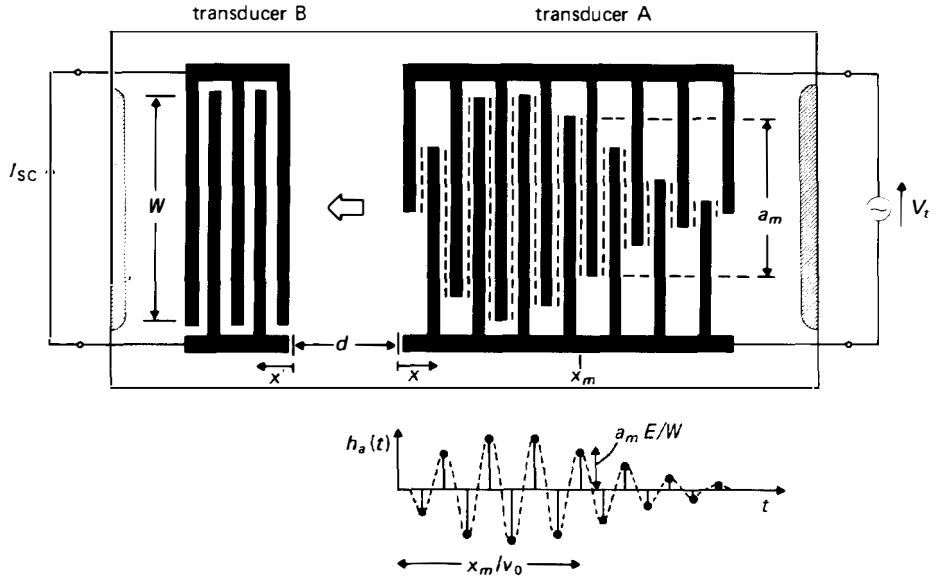

FIGURE 4.3. Apodised transducer and its impulse response.

longest source has a length W, equal to the aperture of transducer B. Consider first the surface wave beam generated by source m of transducer A. Assuming diffraction to be negligible, this is given by equation (4.1), so that $\psi_s(x) = EV_tC_m \exp[jk_0(x - x_m)]$. If d is the transducer separation, the two coordinates x and x' are related by $x = -x' - d$, so for transducer B this wave becomes an incident wave $\psi_t^{(m)}(x') = \psi_{i0}^{(m)} \exp(-jk_0x')$, with

$$\psi_{i0}^{(m)} = EV_tC_m \exp[-jk_0(x_m + d)]. \tag{4.12}$$

The output current due to this wave is given by equation (4.9), where the beam width w must be equated with the source length a_m in transducer A. Thus the current is

$$I_{sc}^{(m)} = \psi_{i0}^{(m)} a_m E \sum_{n=1}^{M'} C_n' \exp(-jk_0x_n'), \tag{4.13}$$

where transducer B is taken to have M' receiving elements, with polarities C_n' and locations x_n'. Equation (4.13) is the output current due to source m of transducer A. The total current I_{sc} is obtained by summing the contributions due to the M sources in this transducer, giving

$$I_{sc} = WV_t \exp(-jk_0d)\left[E \sum_{n=1}^{M'} C_n' \exp(-jk_0x_n')\right] H_a(\omega), \tag{4.14}$$

where

$$H_a(\omega) = E \sum_{m=1}^{M} \frac{a_m}{W} C_m \exp(-jk_0x_m). \tag{4.15}$$

In equation (4.14), the term in square brackets is, by comparison with equation (4.2), the frequency response of transducer B. The term $H_a(\omega)$ can be taken as the frequency

response of transducer A, which is apodised. Thus the device response is essentially the product of the two transducer responses. Equation (4.15) is consistent with the frequency response defined for an unapodised transducer, as can be seen by setting $a_m = W$. It should be noted that this formulation is valid only if transducer B is unapodised. It has also been assumed that the transducers do not reflect incident surface waves; this is found to be a reasonable assumption for many devices, provided the transducers are connected to zero electrical impedances, as they are in Figure 4.3.

The influence of the geometry of the apodised transducer is shown more clearly by considering its impulse response $h_a(t)$, which can be defined as the inverse Fourier transform of $H_a(\omega)$. Noting that $k_0 = \omega/v_0$, where v_0 is the free-surface velocity, independent of ω, equation (4.15) gives

$$h_a(t) = E \sum_{m=1}^{M} \frac{a_m C_m}{W} \delta(t - x_m/v_0) \tag{4.16}$$

assuming E to be constant. Thus the impulse response is a sequence of delta functions at times corresponding to the element locations, with amplitudes given by the electrode overlaps a_m, as shown in the lower part of Figure 4.3. Physically this form for the impulse response is unrealistic because E is in fact a function of ω; however, if equation (4.16) is transformed to the frequency domain, taking E to be constant, the result is a good approximation in the region of the fundamental frequency response.

In view of this, it is convenient to consider an alternative definition of the impulse response, denoted $\tilde{h}_a(t)$, such that the harmonic responses in the frequency domain are eliminated. Thus the Fourier transform of $\tilde{h}_a(t)$ is the same as the transform of $h_a(t)$ for $\omega < 2\omega_c$, but is zero for $\omega > 2\omega_c$, with $\omega_c = \pi v_0/p$ as before. The form of $\tilde{h}_a(t)$ can be obtained from the equations of sampling theory, summarised later in Section 8.1.2 of Chapter 8. It is assumed that the element lengths a_m do not change rapidly, so that we can define a smooth function $a(x)$ such that $a_m = a(x_m)$, with the element locations given by $x_m = mp$. The smooth nature of $a(x)$ is expressed by requiring its Fourier transform $\bar{a}(\beta)$ to be zero for $|\beta| > \omega_c/v_0$. This is found to give

$$\tilde{h}_a(t) = \frac{\omega_c E}{\pi W} a(v_0 t) \cos(\omega_c t). \tag{4.17}$$

This is an amplitude-modulated sinusoid, with peaks and troughs at the locations $t = x_m/v_0$ of the delta functions comprising $h_a(t)$. At these locations, $\tilde{h}_a(t)$ is proportional to the amplitudes of the delta-functions. The broken line in the lower part of Figure 4.3 shows the function $\pi\tilde{h}_a(t)/\omega_c$. It is often convenient to regard $\tilde{h}_a(t)$ as the effective impulse response of the transducer [81], because the harmonics are relatively insignificant.

This formulation leads to a simple design prescription, asuming that some required frequency response for the transducer has been given. The frequency response is Fourier transformed to the time domain. Assuming that this yields an amplitude-modulated carrier, the transducer elements are placed at locations

corresponding to the peaks and troughs of this waveform, and their lengths (the electrode overlaps) are made proportional to the amplitude at these points. For example, if the frequency response is to be constant within a specified band and zero outside this band, the apodisation function $a(x)$ is required to have the form $(\sin Ax)/(Ax)$, where A is a constant, and the geometry of the transducer is illustrated by Figure 1.4. The design procedure is thus very versatile and, in principle, straightforward. Further details will be given in Chapter 8, where it will be shown that the impulse response may have phase modulation as well as amplitude modulation.

4.2. DISCUSSION OF SECOND-ORDER EFFECTS AND METHODS OF ANALYSIS

Although the delta-function model described above gives a very useful first-order method of transducer analysis, it fails to account for a number of second-order effects that are often significant in practice. In addition some important transducer properties, notably the element factor and the transducer admittance, are not given by this model. A more detailed analysis will be given below, but it is convenient to consider first the variety of transducer types and the relevant second-order effects, in order to clarify the requirements for transducer analysis. We also discuss some of the theoretical models that are used.

An important second-order effect is the reflection of incident surface waves by a transducer. In a device using two transducers, the output transducer will in general produce a reflected wave, which is then reflected a second time by the input transducer. Thus, a reflected wave reaches the output transducer after traversing the substrate three times, giving an unwanted output signal known as the *triple-transit* signal. There are also spurious signals due to additional reflections, but these are usually insignificant. For C.W. excitation of the input transducer, the triple-transit signal causes the device output, as a function of frequency, to exhibit a ripple. If a short pulse is applied to the input transducer, the triple-transit signal takes the form of an unwanted output pulse following the main pulse. The two pulses often overlap, but are resolved if the transducer separation is large enough.

In practice there are two particular considerations that affect the reflection coefficient: electrode interactions, and the value of the electrical load connected to the transducer. Suppose initially that the transducer is shorted, or connected to a source with zero impedance. In this situation, the transducer can reflect surface waves because the electrodes cause mechanical and electrical perturbations of the surface. This effect is here called *electrode interactions*, though the term "mechanical and electrical loading" (MEL) is also used. Each electrode can be considered to reflect the surface waves. Although the perturbation is small, the reflected waves add coherently if the electrode spacing equals half the wavelength, and the total reflection coefficient can therefore be quite large. It is found that this also distorts the frequency response of the transducer. The transducers of Section 4.1 have two electrodes per period, as shown in Figure 4.4(a), and consequently the interactions can be strong at the fundamental centre frequency ω_c. For a strongly piezoelectric substrate material, such

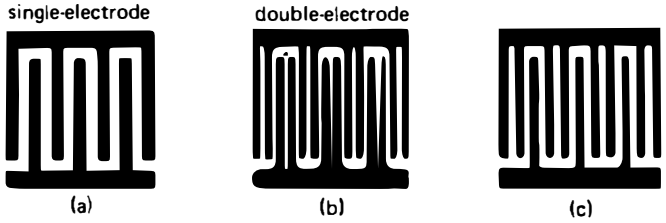

FIGURE 4.4. Types of uniform transducer.

as lithium niobate, significant interactions occur if the number of electrodes, N, is such that $N\Delta v/v > 1$, where $\Delta v/v$ is the fractional velocity change due to a continuous metal film. To overcome this, *multi-electrode* transducers, such as those in Figure 4.4(b) and (c), are often used [82, 83]. Here there are more than two electrodes per period, so that strong reflections can occur only at frequencies well removed from the centre frequency ω_c. The simpler transducer of Figure 4.4(a) is often called a *single-electrode* transducer, while the transducer of Figure 4.4(b) is a *double-electrode* transducer.

Practical devices are usually designed such that electrode interactions are weak, since this enables a relatively straightforward design procedure to be used. Thus, for practical purposes, an analysis that neglects electrode interactions is usually adequate. This is the case for all of the analysis in this chapter, including the delta-function analysis of Section 4.1. In the sections to follow, the "quasi-static approximation" is used, with the consequence that the analysis neglects electrode interactions. However, Appendix E gives a second-order analysis which does not use this approximation, and describes electrode interactions in more detail.

In the above discussion the transducer was taken to be connected to an electrical impedance of zero, and, assuming electrode interactions are weak, its reflection coefficient is small in this situation. However, significant reflectivity can still arise when the load impedance is finite. For example, if the transducer is electrically matched to a load, thus optimising its conversion efficiency, the power reflection coefficient is theoretically $\frac{1}{4}$, giving a triple-transit signal too large for most applications. This large reflection coefficient is a consequence of the bidirectional nature of the transducer. The usual remedy is to avoid a close match of the impedances, accepting the consequent loss of efficiency. However, there are several special types of transducer that are essentially uni-directional, giving simultaneously a low reflection coefficient and good conversion efficiency. These will be described in Chapters 5 and 7.

In addition to its influence on the reflection coefficient, the use of a finite external impedance also affects the frequency response of a device to some extent. This is known as the "circuit effect", and is often significant for devices whose responses are accurately specified.

Some further second-order effects are associated with the electrostatic charge density on the transducer, that is, the charge density for unit applied voltage, calculated with the piezoelectric effect ignored. This function can be regarded, to a good approximation, as a distributed source of surface waves, thus giving the

surface-wave amplitude generated by the transducer. With some restrictions, this approach enables the transducer response to be expressed in terms of an array factor and an element factor, as in Section 4.1, and yields an expression for the element factor, E. This procedure is necessary in order to evaluate the levels of the harmonic responses. The charge density on any one electrode can be regarded as a surface wave source associated with that electrode; however the charge density is affected by the configuration of several neighbouring electrodes on either side, which thus affect the associated surface wave amplitude. This is known as the *neighbour effect*. Fortunately, the neighbour effect can be allowed for implicitly by re-defining the surface wave component associated with each electrode, and so need not be considered explicitly. The transducers in Figure 4.4 are also affected by "end effects", that is, the electrodes near the ends have charge densities somewhat different to those in the centre. However, it is shown in Section 4.5.1 that end effects can be virtually eliminated by adding "guard" electrodes at each end of the transducer. Finally, it is noted that some "withdrawal-weighted" transducers have structures too irregular to allow the use of an array factor and element factor, but the response may nevertheless be deduced from the electrostatic solution.

Another complication is the excitation of bulk waves in addition to the intended surface waves. The bulk waves usually propagate away from the surface and therefore do not excite a receiving transducer very strongly, though it is often necessary to ensure this by roughening the rear surface of the substrate, suppressing specular reflections. Bulk waves travelling almost parallel to the surface reach the output transducer directly, and can be of some practical concern. In many devices, a multi-strip coupler is used to discriminate against them.

It will be seen that there is a considerable variety of transducer types and the behaviour is affected by a variety of second-order effects. In consequence, a variety of methods have been used for transducer analysis. The delta-function model described above is widely used because of its simplicity, despite its limitations — notably, the inability to calculate the transducer admittance and reflection coefficient, and, for a two-transducer device, the insertion loss. These limitations were largely overcome by the "crossed-field" network model introduced by Smith *et al.* [84–87], drawing an analogy between the surface-wave transducer and an array of bulk wave transducers. Each electrode (or, sometimes, pair of electrodes) in the surface wave transducer was replaced by an equivalent network, so that the response of a complex transducer could be found by analysing an array of networks, using conventional network analysis [79, 84]. The original model excluded electrode interactions and bulk wave excitation, and did not correctly allow for electrostatic effects. However, it was shown later that interactions could be modelled by including a repetitive impedance mis-match [85, 88, 89]. Also, electrostatic effects could be included by finding the electrostatic solution first and then incorporating it into the network model [90].

More rigorously, a number of theoretical approaches have been explored, including perturbation theory which has been applied to the analysis of both transducers [91] and multi-strip couplers. Another approach, more closely related to the analysis in this chapter, is based on the effective permittivity described in

Chapter 3. For transducer analysis, this concept was used in the Green's function method of Milsom *et al.* [92–94], where the Green's function was derived from the effective permittivity, as described in Section 3.4. The definition of the effective permittivity is such that, if applied rigorously, it implicitly allows for electrode interactions, bulk waves and electrostatic effects, though mechanical loading due to the electrodes is excluded. This method is therefore very versatile, though its complexity makes it somewhat inconvenient. The effective permittivity has also been applied to the analysis of multi-strip couplers, making use of Ingebrigtsen's approximation.

The analysis given below in this chapter is an approximate form of the Green's function method [95]. An approximate Green's function described in Section 3.4 is used, assuming bulk wave excitation to be negligible. The analysis also uses the quasi-static approximation, and thus neglects electrode interactions. The resulting method is relatively straightforward, giving simple results valid for a wide range of transducer types, and correctly allows for electrostatic effects. In most practical devices, electrode interactions and bulk wave excitation are relatively insignificant, and these topics are described in Appendices E and F, respectively. Diffraction of the surface waves is ignored in this chapter, but will be described in Chapter 6. Some fundamental relationships, derived from Auld's reciprocity relation, are given in Appendix B.

4.3. ANALYSIS FOR A GENERAL ARRAY OF ELECTRODES

In this section we consider an array of electrodes on the surface of a piezoelectric half-space, as illustrated in Figure 4.5(a). The analysis is based on the Green's function described in Section 3.4, and therefore excludes mechanical loading due to the electrodes. Section 3.4 also assumes the potential and charge density to be invariant in one direction in the surface, and to comply with this the aperture W in Figure 4.5(a) is assumed to be large, so that distortions near the ends of the electrodes can be neglected. Surface-wave diffraction is also neglected. It is assumed that the only acoustic wave present is a non-leaky piezoelectric Rayleigh wave, thus excluding bulk wave excitation. The electrodes are taken to have negligible resistivity.

The electrode voltages are all taken to have the same frequency ω, but are otherwise arbitrary. This enables the results to be used for analysis of multi-strip couplers, as well as transducers. The transducer analysis is given in the following sections of this chapter, while the multi-strip coupler analysis is given in Chapter 5.

4.3.1. The Quasi-Static Approximation

In Section 3.4 it was shown that the potential $\phi(x, \omega)$ and charge density $\sigma(x, \omega)$ at the surface of a piezoelectric half-space are related by a Green's function $G(x, \omega)$. Here $\phi(x, \omega)$ and $\sigma(x, \omega)$ are both proportional to $\exp(j\omega t)$, with this factor implicit. Since the only acoustic wave present is assumed to be a Rayleigh wave, $G(x, \omega)$ can be approximated as the sum of an electrostatic term $G_e(x)$ and a surface wave term $G_s(x, \omega)$, as in equation (3.48), so that

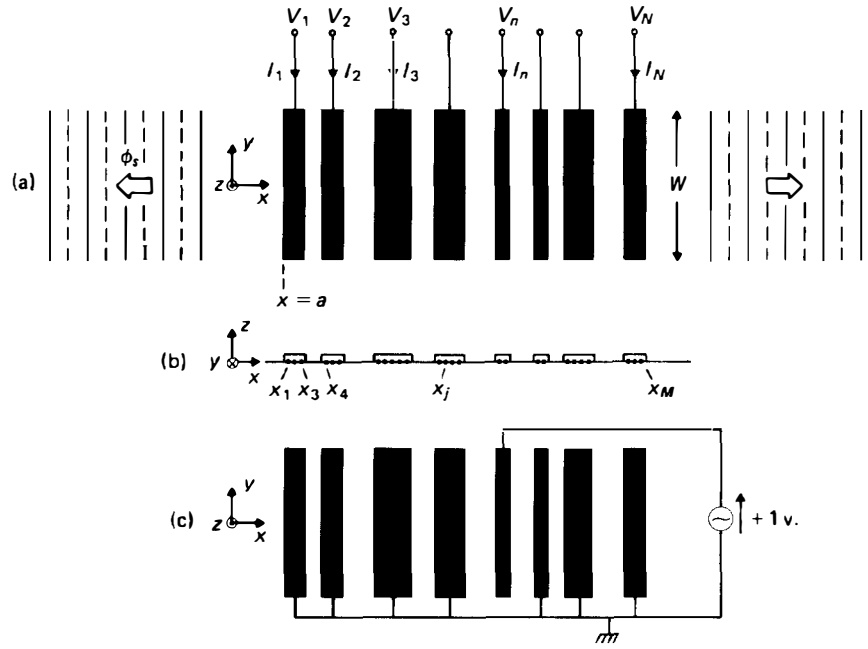

FIGURE 4.5. Generalised array of electrodes.

$$\phi(x, \omega) = [G_e(x) + G_s(x, \omega)] * \sigma(x, \omega), \tag{4.18}$$

where the asterisk indicates convolution with respect to x. For convenience, the axis notation has been changed here, so that new coordinates x, y, z replace the earlier coordinates x_1, x_2, x_3. Thus the piezoelectric now occupies the region $z < 0$, and the surface waves propagate in the $\pm x$ directions. The two components of the Green's function are

$$G_e(x) = -\frac{\ln |x|}{\pi(\varepsilon_0 + \varepsilon_p^T)}, \tag{4.19}$$

and

$$G_s(x, \omega) = j\Gamma_s \exp(-jk_0|x|), \tag{4.20}$$

where $k_0 > 0$ is the wavenumber for surface wave propagation on a free surface at frequency ω. The constant ε_p^T is given by equation (3.37) with the elements ε_{ij} defined at constant stress, and the constant Γ_s is, from equation (3.39),

$$\Gamma_s \approx \frac{1}{\varepsilon_0 + \varepsilon_p^T} \frac{v_0 - v_m}{v_0}, \tag{4.21}$$

where v_0 and v_m are respectively the surface wave velocities for a free surface and for a metallised surface.

Since the electrode resistivity is assumed to be negligible, each electrode will be an

equipotential, and $\phi(x, \omega)$ must be equal to the electrode voltage at all points on the electrode. The charge density $\sigma(x, \omega)$ must be zero on all unmetallised regions. Using these boundary conditions and the equations given above, the surface potential and charge density are determined everywhere if the electrode voltages are specified.

At points remote from the electrodes, the surface potential is primarily the potential $\phi_s(x, \omega)$ associated with the surface waves generated by the structure. For example, consider the unmetallised region $x < a$, assuming that the electrodes are present only for $x \geqslant a$. Since $\sigma(x, \omega)$ is zero for $x < a$, the electrostatic term $G_e(x)$ in equation (4.18) gives a potential decaying with distance in this region. The surface-wave potential $\phi_s(x, \omega)$ can therefore be identified with $G_s(x, \omega) * \sigma(x, \omega)$, with $G_s(x, \omega)$ given by equation (4.20). Defining $\bar{\sigma}(\beta, \omega)$ as the Fourier transform of $\sigma(x, \omega)$, with ω held constant in the Fourier integral, the surface-wave potential is found to be

$$\phi_s(x, \omega) = j\Gamma_s \bar{\sigma}(k_0, \omega) \exp(jk_0 x), \quad \text{for } x < a \tag{4.22}$$

where the modulus sign in equation (4.20) has disappeared because $\sigma(x, \omega)$ is zero for $x < a$. Thus the surface-wave potential is given by the Fourier transform of the charge density. Although bulk wave excitation has been neglected here, equation (4.22) is still valid when bulk waves are excited, as shown in Appendix B, equation (B.30). In fact, equation (4.22) is derived indirectly from equation (B.30), since the latter was used in Section 3.4 to derive the surface wave Green's function $G_s(x, \omega)$.

It should be noted that $\bar{\sigma}(k_0, \omega)$ is not the Fourier transform of $\sigma(x, \omega)$ in the usual sense, because k_0 is not an independent parameter. If ω is changed, $\sigma(x, \omega)$ will in general change, so the Fourier integral must be calculated separately for each ω. For clarity, β is used here as the independent variable in the transform, while k, with various subscripts, refers to wavenumbers of propagating waves.

Although the above equations can be solved to obtain the surface potential and charge density, the calculation is generally very complex. Here the *quasi-static approximation* [95] is introduced in order to simplify the solution. The charge density $\sigma(x, \omega)$ is assumed to be dominated by an electrostatic term $\sigma_e(x, \omega)$, defined as the charge density obtained when acoustic wave excitation is ignored. Thus, from equation (4.18), $\sigma_e(x, \omega)$ is the solution of

$$\phi_e(x, \omega) = G_e(x) * \sigma_e(x, \omega). \tag{4.23}$$

Here $\phi_e(x, \omega)$ is a new surface potential, equal to the specified electrode voltage whenever x is on an electrode, and $\sigma_e(x, \omega) = 0$ on all unmetallised regions. Note that $\sigma_e(x, \omega)$ is independent of ω if the electrode voltages are independent of ω, and $\sigma_e(x, \omega)$ is zero if the electrode voltages are all the same. The total charge density is now taken to be

$$\sigma(x, \omega) \approx \sigma_e(x, \omega) + \sigma_a(x, \omega), \tag{4.24}$$

where $\sigma_a(x, \omega)$ is a relatively small contribution due to the piezoelectric effect; it can be regarded as a regenerated term due to the acoustic waves present. The surface potential $\phi(x, \omega)$ is given by equation (4.18), using equation (4.24) for $\sigma(x, \omega)$. On the right there are now four terms, but a term $G_s(x, \omega) * \sigma_a(x, \omega)$ is small, and can

be omitted; both $G_s(x, \omega)$ and $\sigma_a(x, \omega)$ become zero if there is no piezoelectric coupling. We thus have, in the quasi-static approximation,

$$\phi(x, \omega) = [G_e(x) + G_s(x, \omega)] * \sigma_e(x, \omega) + G_e(x) * \sigma_a(x, \omega). \quad (4.25)$$

Given the function $\sigma_e(x, \omega)$, this equation, together with the boundary conditions, determines the acoustic charge density $\sigma_a(x, \omega)$, as discussed further in Section 4.3.3 below. Also, $\sigma_e(x, \omega)$ is determined by equation (4.23). Hence the total charge density, equation (4.24), and the surface potential, equation (4.25), are determined. The solution is approximate because one term was omitted in deriving equation (4.25). However, we define $\sigma_a(x, \omega)$ such that equation (4.25) is exactly true; it then follows that the charge density is not exactly the sum of $\sigma_e(x, \omega)$ and $\sigma_a(x, \omega)$, so that equation (4.24) is approximate.

As explained earlier, the potential $\phi_s(x, \omega)$ of a surface wave generated by the electrodes can be obtained by omitting terms arising from the electrostatic Green's function $G_e(x)$. Using equation (4.25) the surface-wave potential for $x < a$, to the left of the structure, is found to be

$$\phi_s(x, \omega) = j\Gamma_s \bar{\sigma}_e(k_0, \omega) \exp(jk_0 x), \quad \text{for } x < a, \quad (4.26)$$

where we define $\bar{\sigma}_e(\beta, \omega)$ as the Fourier transform of $\sigma_e(x, \omega)$. This is the same as the more accurate result of equation (4.22), except that $\bar{\sigma}(k_0, \omega)$ is replaced by $\bar{\sigma}_e(k_0, \omega)$. This change simplifies the analysis considerably, as can be seen for example by considering excitation by a two-terminal transducer. For this case it is sufficient to take the electrode voltages to be ± 1, and thus to be independent of the frequency ω (a term $\exp(j\omega t)$ is implicit). This implies that the electrostatic charge density $\sigma_e(x, \omega)$ is independent of ω, and hence the surface wave amplitude for all ω can be deduced by evaluating $\sigma_e(x, \omega)$ at $\omega = 0$. For this reason, the approximation is described as "quasi-static".

4.3.2. Electrostatic Equations and Charge Superposition

The electrostatic charge density $\sigma_e(x, \omega)$ is determined by equation (4.23), with the boundary conditions that the potential $\phi_e(x, \omega)$ is equal to the electrode voltage whenever x is on an electrode, and $\sigma_e(x, \omega)$ is zero on all unmetallised regions. An elegant technique for finding $\sigma_e(x, \omega)$ has been given by Milsom *et al.* [93], who in fact used it for the piezoelectric case. The application to the electrostatic problem is discussed here. We define a set of M points x_j, as shown in Figure 4.5(b). The points exist only on the electrodes, where they have a small spacing Δx. The electrostatic equation (4.23) is written as

$$\phi_e(x_i, \omega) = \sum_{j=1}^{M} A_{ij} \sigma_e(x_j, \omega), \quad (4.27)$$

which will be identical to equation (4.23) in the limit when Δx vanishes and M becomes infinite. The obvious choice for the coefficients A_{ij} is $\Delta x G_e(x_i - x_j)$, but for finite Δx this is infinite when $i = j$, as can be seen from equation (4.19). A suitable choice for A_{ij} is therefore

$$A_{ij} = \tfrac{1}{2}\Delta x[G_e(x_i - x_j + \tfrac{1}{2}\Delta x) + G_e(x_i - x_j - \tfrac{1}{2}\Delta x)]. \quad (4.28)$$

This matrix takes account of the electrode geometry, since the points x_j exist only on the electrodes. Owing to the symmetry of $G_e(x)$, A_{ij} is symmetrical, so that $A_{ji} = A_{ij}$. We may now invert equation (4.27) to express $\sigma_e(x, \omega)$ in terms of $\phi_e(x, \omega)$:

$$\sigma_e(x_i, \omega) = \sum_{j=1}^{M} B_{ij}\phi_e(x_j, \omega), \quad (4.29)$$

where B_{ij} is the reciprocal of the matrix A_{ij}. Since A_{ij} is symmetrical, it follows that B_{ij} is also symmetrical:

$$B_{ji} = B_{ij}. \quad (4.30)$$

In equation (4.29) all the $\phi_e(x_j, \omega)$ are equal to known electrode voltages, since the points x_j exist only on the electrodes. Thus the potential in the inter-electrode gaps, which is not known *a priori*, is not required. The condition that $\sigma_e(x, \omega)$ should be zero in the gaps is implied by equation (4.27), because the summation excludes points not on the electrodes.

Charge Superposition. A useful principle for simplifying the determination of $\sigma_e(x, \omega)$ can be found by considering the arrangement shown in Figure 4.5(c). Here the electrodes are as in Figure 4.5(a), but now electrode n has unit voltage while all the other electrodes are grounded. The electrostatic charge density for this case is denoted $\varrho_{en}(x)$, and is real and independent of frequency. In general there will be charges present on all the electrodes, not just on electrode n. To find $\varrho_{en}(x)$, we define an electrode polarity function $\hat{p}_n(x)$ by

$$\begin{aligned} \hat{p}_n(x) &= 1 \quad \text{if } x \text{ is on electrode } n, \\ &= 0 \quad \text{for other } x. \end{aligned} \quad (4.31)$$

For a point x_j on any electrode, the potential in Figure 4.5(c) is $\hat{p}_n(x_j)$, and hence from equation (4.29) the electrostatic charge density is

$$\varrho_{en}(x_i) = \sum_{j=1}^{M} B_{ij}\hat{p}_n(x_j) \quad (4.32)$$

with $\varrho_{en}(x) = 0$ on the unmetallised regions.

The charge superposition principle states that, when some arbitrary set of voltages is applied to the electrodes, the charge density is given by a linear combination of the functions $\varrho_{en}(x)$ due to individual electrodes. Thus, for Figure 4.5(a), where the electrode voltages are V_n, the electrostatic charge density is

$$\sigma_e(x, \omega) = \sum_{n=1}^{N} V_n\varrho_{en}(x). \quad (4.33)$$

This equation follows directly from equation (4.29). It is of considerable practical value, since $\sigma_e(x, \omega)$ can be evaluated for any set of electrode voltages V_n, once the

functions $\varrho_{en}(x)$ are known. The superposition principle is well known in electrostatics, and is discussed in more detail by, for example, Ramo *et al.* [96]. It should be noted that the charge density must be zero if the surface potential is independent of x, since for this case there is no electric field. It follows that $\sigma_e(x, \omega)$ is unaffected if a constant is added to all the V_n in equation (4.33).

Evaluation of the Electrostatic Charge Density. The electrostatic charge density $\sigma_e(x, \omega)$ can be expressed analytically if the electrodes are regular, that is, if they have the same width and have uniform spacing. This solution is described in Section 4.5 below, where it is used to deduce transducer behaviour. Analytic solutions are also known for some simple cases, where the structure has either 2 or 3 electrodes [97]. In general, however, numerical techniques must be used. For several reasons, notably analysis of withdrawal-weighted transducers, these techniques have been investigated quite extensively. The literature refers to two-terminal transducers, where each electrode voltage takes one of two values; however, the methods can be applied directly when the voltages are all different.

Numerical techniques were first used by Hartmann and Secrest [98] to investigate end effects. The method made use of the relation between charge density and potential in the β-domain, given by equation (3.12) of Chapter 3. The boundary conditions (specified voltages on the electrodes and zero charge density in the gaps) are given in the x-domain, so an iterative technique involving Fourier transformation was used. Another method is based on the relationship shown in equation (4.29), which expresses the charge density in terms of the known electrode voltages; the matrix A_{ij} is obtained directly from the electrostatic Green's function [equation (4.28)], and is inverted to give the coefficients B_{ij} required in equation (4.29). A particular feature that can cause difficulty is that the charge density is infinite at the electrode edges. In view of this Milsom *et al.* [93] refined the method by using unequal spacing for the points x_j.

Several authors have used a method in which the charge density on each electrode is written as a polynomial with unknown coefficients. Substituting into equation (4.27) gives a set of simultaneous equations for the electrode potentials, and these can be solved for the polynomial coefficients. Quite good accuracy can be obtained with only three coefficients per electrode [99], and excellent results can be obtained using Chebychev polynomials [90, 100]. Tabulated results [90, 100] can be used to analyse a variety of cases, making use of the superposition principle mentioned above.

Another method replaces the actual electrodes by a fine grid of regular electrodes, for which the charge density is known analytically, applying boundary conditions of zero charge or specified potential as appropriate [101].

4.3.3. Current Entering One Electrode

The current entering one electrode can be found from the charge density on it, and we first consider the charge density in more detail, showing that $\sigma_a(x, \omega)$ can be expressed in terms of $\sigma_e(x, \omega)$. The electrostatic term $\sigma_e(x, \omega)$ is defined as the solution of equation (4.23), which involves a potential $\phi_e(x, \omega)$. The actual potential $\phi(x, \omega)$ is given by equation (4.25), which can be seen to include a term equal to

$\phi_e(x, \omega)$. Since $\phi(x, \omega)$ and $\phi_e(x, \omega)$ must be equal when x is on an electrode, the remaining terms in equation (4.25) must be zero at such points, so that

$$[G_s(x, \omega) * \sigma_e(x, \omega) + G_e(x) * \sigma_a(x, \omega)]_{x_j} = 0. \tag{4.34}$$

This equation relates $\sigma_a(x, \omega)$ to $\sigma_e(x, \omega)$. It is convenient to define an acoustic potential $\phi_a(x, \omega)$ by the expression

$$\phi_a(x, \omega) = G_s(x, \omega) * \sigma_e(x, \omega). \tag{4.35}$$

This potential is associated with acoustic wave excitation, and is zero if the material is not piezoelectric. Equation (4.34) can thus be written

$$[G_e(x) * \sigma_a(x, \omega)]_{x_i} = -\phi_a(x_j, \omega). \tag{4.36}$$

This has the same form as equation (4.23), and may therefore be expressed in a form similar to equation (4.27). The charge density $\sigma_a(x, \omega)$ is therefore, by analogy with equation (4.29),

$$\sigma_a(x_i, \omega) = -\sum_{j=1}^{M} B_{ij}\phi_a(x_j, \omega), \tag{4.37}$$

where B_{ij} is the inverse of the matrix A_{ij} defined in equation (4.28). For values of x on the electrodes, equation (4.37) gives $\sigma_a(x, \omega)$ exactly, in the limit $\Delta x \to 0$. For other x, $\sigma_a(x, \omega)$ is of course zero. Thus, using equation (4.35) for $\phi_a(x, \omega)$, $\sigma_a(x, \omega)$ can be deduced from $\sigma_e(x, \omega)$.

The current I_n flowing into electrode n is found by integrating the total charge density over the surface of the electrode, and then differentiating with respect to time. Thus

$$I_n = j\omega W \int_n [\sigma_e(x, \omega) + \sigma_a(x, \omega)]\,\mathrm{d}x, \tag{4.38}$$

where the integral is taken over electrode n. The current is taken as the sum of two terms,

$$I_n = I_{en} + I_{an}, \tag{4.39}$$

where I_{en} and I_{an} are respectively the contributions due to $\sigma_e(x, \omega)$ and $\sigma_a(x, \omega)$. Thus

$$I_{en} = j\omega W \int_n \sigma_e(x, \omega)\,\mathrm{d}x. \tag{4.40}$$

It is assumed that $\sigma_e(x, \omega)$ can be evaluated, so this contribution will not be considered further here. The acoustic contribution can be written

$$I_{an} = j\omega W \int_{-\infty}^{\infty} \hat{p}_n(x)\,\sigma_a(x, \omega)\,\mathrm{d}x, \tag{4.41}$$

where $\hat{p}_n(x)$, defined by equation (4.31), is unity on electrode n and zero elsewhere. Since the integrand here is zero in the unmetallised regions, the integral can be expressed as discrete sum using the points x_j, so that

$$\begin{aligned} I_{an} &= j\omega W \sum_{j=1}^{M} \hat{p}_n(x_j)\,\sigma_a(x_j, \omega)\,\Delta x \\ &= -j\omega W \Delta x \sum_{i=1}^{M} \phi_a(x_i, \omega) \sum_{j=1}^{M} \hat{p}_n(x_j)\, B_{ji}, \end{aligned} \tag{4.42}$$

where equation (4.37) has been used for $\sigma_a(x_j, \omega)$ and the summations have been re-ordered. Now, since B_{ij} is symmetrical, comparison with equation (4.32) shows that the sum over j in equation (4.42) can be identified as $\varrho_{en}(x_i)$. Hence

$$I_{an} = -j\omega W \sum_{i=1}^{M} \phi_a(x_i, \omega)\, \varrho_{en}(x_i)\, \Delta x$$

or, taking the limit as $\Delta x \to 0$,

$$I_{an} = -j\omega W \int_{-\infty}^{\infty} \varrho_{en}(x)\, \phi_a(x, \omega)\, \mathrm{d}x \tag{4.43}$$

since $\varrho_{en}(x)$ is zero in the unmetallised regions.

4.3.4. Evaluation of the Acoustic Potential

The acoustic potential $\phi_a(x, \omega)$ in equation (4.43) is defined in terms of $\sigma_e(x, \omega)$ by equation (4.35). For the analysis later we will need an expression involving $\bar{\sigma}_e(\beta, \omega)$, the Fourier transform of $\sigma_e(x, \omega)$, and this is derived here. From equation (4.35),

$$\phi_a(x, \omega) = G_s(x, \omega) * \sigma_e(x, \omega),$$

where $G_s(x, \omega)$ is given by equation (4.20). Thus,

$$\begin{aligned}\phi_a(x, \omega) &= j\Gamma_s \int_{-\infty}^{x} \sigma_e(x', \omega)\, \mathrm{e}^{-jk_0(x-x')}\, \mathrm{d}x' \\ &\quad + j\Gamma_s \int_{x}^{\infty} \sigma_e(x', \omega)\, \mathrm{e}^{jk_0(x-x')}\, \mathrm{d}x'.\end{aligned} \tag{4.44}$$

If the electrodes are present only for $x \geqslant a$, as in Figure 4.5(a), this equation gives $\phi_a(x, \omega) = j\Gamma_s \bar{\sigma}_e(k_0, \omega) \exp(jk_0 x)$ for the region $x < a$ to the left of the structure. Comparison with equation (4.26) shows that $\phi_a(x, \omega)$ is equal to the surface wave potential $\phi_s(x, \omega)$ for $x < a$, and this is also found to be true for the unmetallised region to the right of the structure.

Equation (4.44) may be re-arranged using the step function $U(x)$, which is equal to 1 for $x > 0$ and to zero for $x < 0$. Thus,

$$\begin{aligned}\phi_a(x, \omega) &= j\Gamma_s\, \mathrm{e}^{-jk_0x} \int_{-\infty}^{\infty} \sigma_e(x', \omega)\, U(x - x')\, \mathrm{e}^{jk_0x'}\, \mathrm{d}x' \\ &\quad + j\Gamma_s\, \mathrm{e}^{jk_0x} \int_{-\infty}^{\infty} \sigma_e(x', \omega)\, U(x' - x)\, \mathrm{e}^{-jk_0x'}\, \mathrm{d}x',\end{aligned} \tag{4.45}$$

where the limits are now $\pm\infty$. These integrals may be evaluated by Fourier methods, taking x as a constant. The first integral is the transform of $[\sigma_e(x', \omega)\, U(x - x')]$, from the x'-domain to the β-domain, with the result evaluated at $\beta = -k_0$. A similar method is used for the second integral. The relationships required are given in Appendix A. The transform of $U(x')$ is, from equation (A.38),

$$U(x') \leftrightarrow \pi\delta(\beta) - j/\beta. \tag{4.46}$$

The shifting and scaling theorems, equations (A.10) and (A.9), are used to obtain the transforms of $U(x - x')$ and $U(x' - x)$, and the products in equation (4.45) are transformed using the convolution theorem, equation (A.20). With $\bar{\sigma}_e(\beta, \omega)$ defined as the Fourier transform of $\sigma_e(x, \omega)$, the result obtained is

$$\phi_a(x, \omega) = \tfrac{1}{2}j\Gamma_s \, e^{-jk_0x}[\bar{\sigma}_e(-k_0, \omega) + jF(-k_0)/\pi] + \tfrac{1}{2}j\Gamma_s^* \, e^{jk_0x}[\bar{\sigma}_e(k_0, \omega) - jF(k_0)/\pi], \quad (4.47)$$

where the function $F(\beta)$ is defined by

$$F(\beta) = \bar{\sigma}_e(\beta, \omega) * \frac{(- \quad x)}{\beta}. \quad (4.48)$$

Here the terms $\bar{\sigma}_e(\pm k_0, \omega)$ arise because of the delta-function in equation (4.46). It will be found later that these give the parallel conductance, $G_a(\omega)$, of a transducer. The terms $F(\pm k_0)$, involving a convolution, are due to the j/β term in equation (4.46) and will be found to give the acoustic susceptance $B_a(\omega)$.

4.4. QUASI-STATIC ANALYSIS OF TRANSDUCERS

We now apply the results of Section 4.3 to a two-terminal unapodised transducer such as that shown in Figure 4.6, where each of the electrodes is connected to one of the two bus-bars. The assumptions mentioned at the beginning of Section 4.3 apply here also, and in addition we assume that the bus bars have no effect other than providing electrical connections to the electrodes, with no resistance. The analysis here uses the quasi-static approximation, since this was used for the derivations in Section 4.3. Consequently, electrode interactions are neglected, as discussed in Section 4.2; for example, the analysis predicts that a shorted transducer will not reflect incident surface waves. Another consequence of the approximation is that surface waves are predicted to travel through a shorted transducer with a velocity equal to the free-surface velocity, v_0. In practice, the electrodes cause a small reduction of the

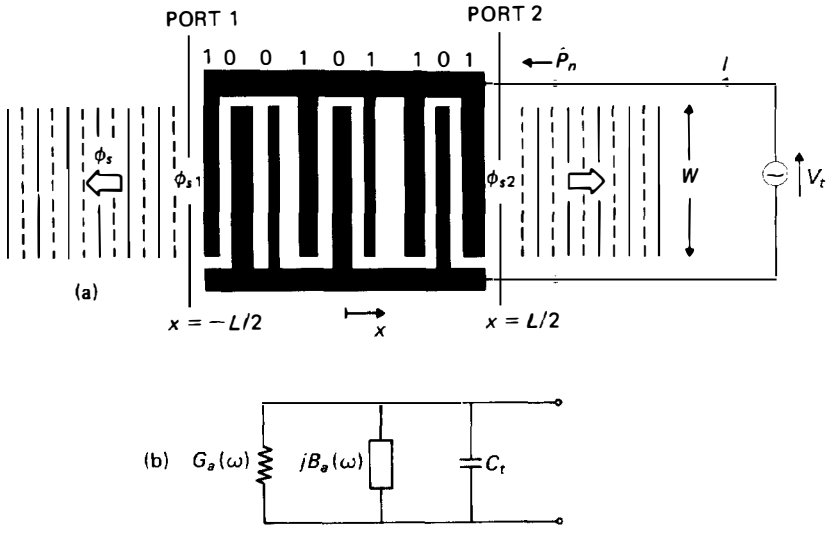

FIGURE 4.6. Two-terminal transducer.

velocity, even when electrode interactions are weak. For regular electrodes, with uniform width and spacing, the velocity change is derived in Section D.2. To allow for this, the results of this section may be modified by replacing the free-surface wavenumber k_0 by k_{sc}, given by equation (D.26).

4.4.1. Launching Transducer

We first consider the transducer of Figure 4.6(a), which is taken to be isolated, that is, there are no incident acoustic waves and the charge density is not affected by the presence of any other electrodes on the surface. A voltage V_t is applied, and the electrostatic part of the charge density is $\sigma_e(x, \omega)$, with Fourier transform $\bar{\sigma}_e(\beta, \omega)$. In the quasi-static approximation, the potential $\phi_s(x, \omega)$ of the surface-wave radiated in the $-x$ direction is, from equation (4.26),

$$\phi_s(x, \omega) = j\Gamma_s \bar{\sigma}_e(k_0, \omega) \exp(jk_0 x).$$

We define $\varrho_e(x) = \sigma_e(x, \omega)/V_t$ as the electrostatic charge density for unit applied voltage. This function is real and independent of frequency. If $\bar{\varrho}_e(\beta)$ is the Fourier transform of $\varrho_e(x)$, we then have

$$\phi_s(x, \omega) = j\Gamma_s V_t \bar{\varrho}_e(k_0) \exp(jk_0 x). \tag{4.49}$$

The transducer has two acoustic ports, and these are taken to be at $x = \pm L/2$. These points are taken to be close to the ends of the transducer, though their precise locations are immaterial. Defining $\phi_{s1}(\omega)$ as the potential of the wave launched at port 1, that is, at $x = -L/2$, we have

$$\phi_{s1}(\omega) = \phi_s(-\tfrac{1}{2}L, \omega) = j\Gamma_s V_t \bar{\varrho}_e(k_0) \exp(-\tfrac{1}{2}jk_0 L). \tag{4.50}$$

The power P_s carried by this wave is, from equation (3.34),

$$P_s = \tfrac{1}{4}\omega W |\phi_{s1}(\omega)|^2/\Gamma_s. \tag{4.51}$$

Similarly, the potential $\phi_{s2}(\omega)$ of the wave launched in the $+x$ direction, measured at port 2 ($x = L/2$), is found to be

$$\phi_{s2}(\omega) = j\Gamma_s V_t \bar{\varrho}_e(-k_0) \exp(-\tfrac{1}{2}jk_0 L). \tag{4.52}$$

Since $\varrho_e(x)$ is real, $\bar{\varrho}_e(-k_0) = \bar{\varrho}_e^*(k_0)$, so that $\phi_{s2}(\omega)$ is essentially the conjugate of $\phi_{s1}(\omega)$. Clearly, the two waves have the same power.

The electrostatic charge density $\varrho_e(x)$ can be evaluated by methods discussed in Section 4.3.2. For a two-terminal transducer, we define an electrode polarity vector $\hat{P}_n$ by

$$\begin{aligned} \hat{P}_n &= 1 \quad \text{if electrode } n \text{ is connected to the upper bus} \\ &= 0 \quad \text{if electrode } n \text{ is connected to the lower bus.} \end{aligned} \tag{4.53}$$

as shown in Figure 4.6(a). For unit voltage across the transducer, the charge density may be found by taking the voltage of electrode n to be $\hat{P}_n$, and hence, using equation (4.33),

$$\varrho_e(x) = \sum_{n=1}^{N} \hat{P}_n \varrho_{en}(x), \tag{4.54}$$

where N is the number of electrodes and $\varrho_{en}(x)$ is the electrostatic charge density associated with unit voltage on electrode n, defined in Section 4.3.2.

4.4.2. Transducer Admittance

When a voltage V_t is applied to an isolated transducer, as in Figure 4.6, the transducer draws a current I, and the ratio I/V_t is the transducer admittance, Y_t. A major part of the current is due to the electrostatic charge density $\sigma_e(x, \omega)$, which is in phase with V_t and gives a capacitive contribution to Y_t. This contribution is usually written explicitly, denoting the capacitance by C_t, so that

$$Y_t(\omega) = G_a(\omega) + jB_a(\omega) + j\omega C_t. \tag{4.55}$$

Here $G_a(\omega)$ and $B_a(\omega)$ are the real and imaginary contributions due to $\sigma_a(x, \omega)$, the acoustic charge density. $G_a(\omega)$ is the conductance, and $B_a(\omega)$ is the acoustic susceptance. The admittance may be represented as an electrical equivalent circuit with these three contributions in parallel, as in Figure 4.6(b).

If I_n is the current entering electrode n from the bus-bar, the transducer current I is given by

$$I = \sum_n \hat{P}_n I_n = j\omega W \sum_n \hat{P}_n \int_n [\sigma_e(x, \omega) + \sigma_a(x, \omega)]\,\mathrm{d}x, \tag{4.56}$$

where equation (4.38) has been used for I_n, and the integral is over electrode n. The electrostatic contribution to I is due to the term $\sigma_e(x, \omega)$ and is equal to $j\omega C_t V_t$. Since $\sigma_e(x, \omega) = V_t \varrho_e(x)$, we have

$$C_t = W \sum_n \hat{P}_n \int_n \varrho_e(x)\,\mathrm{d}x, \tag{4.57}$$

which is simply the sum of the electrostatic charges on the electrodes connected to one bus, for unit applied voltage.

The acoustic part of the current, due to the $\sigma_a(x, \omega)$ term in equation (4.56), is denoted I_a. The contribution due to electrode n is denoted I_{an}, and is given by equation (4.43). We thus have

$$I_a = \sum_n \hat{P}_n I_{an} = -j\omega W \int_{-\infty}^{\infty} \sum_n \hat{P}_n \varrho_{en}(x)\,\phi_a(x, \omega)\,\mathrm{d}x. \tag{4.58}$$

Using equation (4.54) this can be expressed as

$$I_a = -j\omega W \int_{-\infty}^{\infty} \varrho_e(x)\,\phi_a(x, \omega)\,\mathrm{d}x. \tag{4.59}$$

This expression is, by definition, equal to $V_t[G_a(\omega) + jB_a(\omega)]$. The acoustic potential $\phi_a(x, \omega)$ is given by equation (4.47). The two terms in equation (4.47) involving $\bar{\sigma}_e(\pm k_0, \omega)$ are found to give the real part of I_a, equal to $V_t G_a(\omega)$. The terms involving $F(\pm k_0)$ give the imaginary part, $jV_t B_a(\omega)$. Noting that $\bar{\sigma}_e(k_0, \omega) = V_t \bar{\varrho}_e(k_0)$ and $\bar{\varrho}_e(-k_0) = \bar{\varrho}_e^*(k_0)$, the conductance is found to be

$$G_a(\omega) = \omega W \Gamma_s |\bar{\varrho}_e(k_0)|^2. \tag{4.60}$$

More directly, the conductance can be found by evaluating the surface-wave power generated, using equations (4.50)–(4.52). Since the electrodes are taken to have zero

resistivity, this power is equal to the power extracted from the voltage source, which is $V_i^2 G_a(\omega)/2$, and this gives equation (4.60).

The susceptance $B_a(\omega)$ is found by substituting the $F(\pm k_0)$ terms of equation (4.47) into equation (4.59). After some manipulation, the result obtained is

$$B_a(\omega) = -\frac{\omega W \Gamma_s}{\pi} |\bar{\varrho}_e(k_0)|^2 * \frac{1}{k_0}, \tag{4.61}$$

This is clearly related to $G_a(\omega)$, equation (4.60). Using the fact that $k_0 = \omega/v_0$, where the free-surface velocity v_0 is independent of ω, $B_a(\omega)$ can be related to $G_a(\omega)$ without using the function $\bar{\varrho}_e(k_0)$. The result is [95]

$$B_a(\omega) = -G_a(\omega) * \frac{1}{\pi\omega}. \tag{4.62}$$

This relation is the Hilbert transform of $G_a(\omega)$. Although it has been derived here using the quasi-static approximation, it is in fact much more general than this. The general proof uses the fact that the relation between I and V_t must be causal, that is, if the voltage is zero for $t < 0$, say, then the current must also be zero for $t < 0$. It follows from this that the real and imaginary parts of the admittance are related by the Hilbert transform [102, p. 198]. The proof assumes the admittance to be zero at infinite frequencies, so the capacitive term must be excluded. Thus the acoustic susceptance $B_a(\omega)$ can be obtained from the conductance without further analysis of the transducer itself [103].

4.4.3. Receiving Transducer

We now consider a transducer with a surface wave incident on it. As shown in Figure 4.7(a), the transducer geometry is the same as before, but now the two bus-bars are shorted, and a current I_{sc} flows between them. The incident surface wave has a potential $\phi_i(x, \omega)$, which is taken to be equal to $\phi_{i1}(\omega)$ at port 1 of the transducer, where $x = -\frac{1}{2}L$. Thus, in the absence of the transducer, the potential of the wave would be

$$\phi_i(x, \omega) = \phi_{i1}(\omega) \exp(-jk_0 x) \exp(-\tfrac{1}{2}jk_0 L). \tag{4.63}$$

The transducer electrodes can be taken to be at zero potential, so there must be a distribution of charges present, such that the potential $\phi_i(x, \omega)$ is cancelled at the electrode locations.

To find this charge distribution, we return to equation (4.25), which is the quasi-static relation between potential and charge density. The charge density is $\sigma_e(x, \omega) + \sigma_a(x, \omega)$, but here the electrostatic term $\sigma_e(x, \omega)$ is zero because the electrode voltages are zero. Thus the charge density is $\sigma_a(x, \omega)$, and is related to the surface potential $\phi(x, \omega)$ by

$$\phi(x, \omega) = G_e(x) * \sigma_a(x, \omega). \tag{4.64}$$

The potential of the incident wave, $\phi_i(x, \omega)$, is an additional term which can be

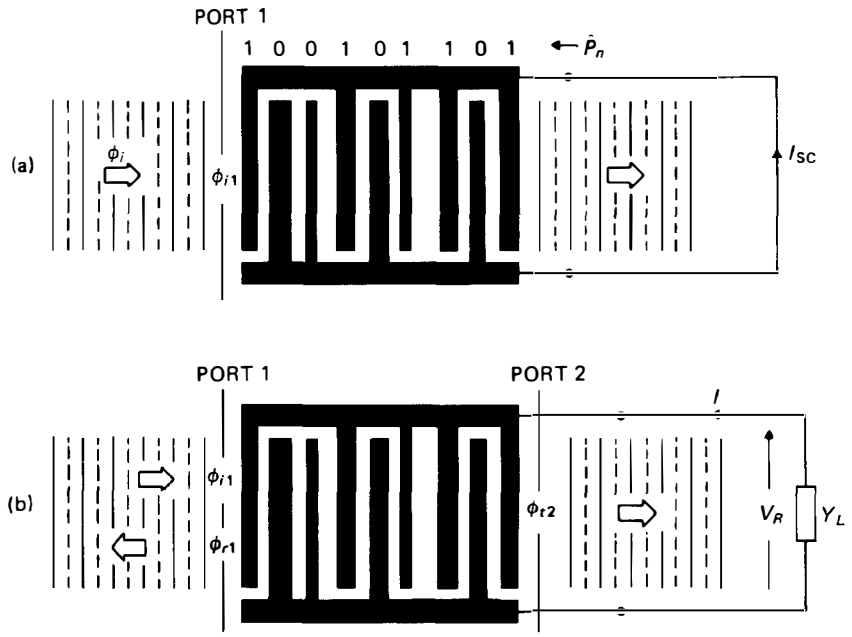

FIGURE 4.7. Reception by a two-terminal transducer.

considered to be due to some remote source whose charge density is not included in equation (4.64). To obtain zero potential on the electrodes we therefore have

$$\phi(x_j, \omega) = [G_e(x) * \sigma_a(x, \omega)]_{x_j} = -\phi_i(x_j, \omega), \tag{4.65}$$

where the points x_j exist only on the electrodes, as before.

A similar equation was found in Section 4.3 above when evaluating the current taken by individual electrodes. Equation (4.65) is the same as equation (4.36), except that $\phi_i(x, \omega)$ has replaced $\phi_a(x, \omega)$. It follows that the current I_{an} entering electrode n is given by equation (4.43), as before, but with $\phi_a(x, \omega)$ replaced by $\phi_i(x, \omega)$, so that

$$I_{an} = -j\omega W \int_{-\infty}^{\infty} \varrho_{en}(x)\, \phi_i(x, \omega)\, \mathrm{d}x. \tag{4.66}$$

The transducer short-circuit current, I_{sc}, is therefore

$$I_{sc} = \sum_n \hat{P}_n I_{an} = -j\omega W \int_{-\infty}^{\infty} \varrho_e(x)\, \phi_i(x, \omega)\, \mathrm{d}x \tag{4.67}$$

where $\varrho_e(x)$ has been introduced by using equation (4.54). Finally, substituting equation (4.63) for $\phi_i(x, \omega)$, we have

$$I_{sc} = -j\omega W \phi_{i1}(\omega) \bar{\varrho}_e(k_0) \exp(-\tfrac{1}{2} j k_0 L). \tag{4.68}$$

Comparing this with equation (4.50) gives a reciprocity relation for the processes of launching and receiving waves at port 1. We have

$$\left[\frac{I_{sc}}{\phi_{i1}(\omega)}\right]_{\text{receive}} = -\frac{\omega W}{\Gamma_s}\left[\frac{\phi_{s1}(\omega)}{V_t}\right]_{\text{launch}}. \tag{4.69}$$

A more general derivation of this equation is given in Appendix B, Section B.5, showing that it is valid when electrode interactions are present, and even when the transducer couples to bulk waves.

4.4.4. Scattering Coefficients

When a surface wave is incident on a transducer there will in general be a reflected wave, and the wave emerging on the other side of the transducer will have an amplitude different from the incident wave. Here we consider the reflection and transmission coefficients, and the conversion of incident power into the power dissipated in an electrical load

For a shorted receiving transducer, the potential associated with the charge density on the electrodes is, in the quasi-static approximation, given by equation (4.64) above. This involves the electrostatic Green's function, and therefore gives a potential localised on and near the transducer. The incident surface wave is therefore not affected by the transducer; there is no reflected wave, and the incident wave passes through the transducer with a velocity v_0, the free-surface velocity, and with no attenuation. Reflections therefore arise only if the transducer is not shorted. In practice, a shorted transducer can in some circumstances give significant reflections owing to electrode interactions as discussed in Section 4.2, but these are neglected here.

We consider a receiving transducer connected to an arbitrary electrical load with admittance Y_L, as in Figure 4.7(b). Since the transducer admittance is Y_t the voltage between the bus-bars, denoted V_R, is found to be

$$\begin{aligned} V_R &= -I_{sc}/(Y_t + Y_L) \\ &= j\omega W \phi_{i1}(\omega)\bar{\varrho}_e(k_0) \exp(-\tfrac{1}{2}jk_0L)/(Y_t + Y_L), \end{aligned} \tag{4.70}$$

where equation (4.68) has been used for the short-circuit current I_{sc}. Generally, Y_L and Y_t are both complex functions of frequency. The charge density on the electrodes now has two contributions — firstly, the charge density obtained for a shorted transducer and, secondly, a charge density arising from the voltage V_R. As discussed above, the first of these does not cause any surface wave excitation. The waves associated with V_R can be calculated as if a voltage V_R were applied to the transducer, with no surface wave incident. The wave radiated to the left, with potential denoted by $\phi_{r1}(\omega)$ at port 1, is therefore given by equation (4.50), with V_t replaced by V_R. Thus

$$\phi_{r1}(\omega) = j\Gamma_s V_R \bar{\varrho}_e(k_0) \exp(-\tfrac{1}{2}jk_0L). \tag{4.71}$$

Using equation (4.70) for V_R, the reflection coefficient at port 1 is

$$r_1(\omega) \equiv \frac{\phi_{r1}(\omega)}{\phi_{i1}(\omega)} = -\frac{\omega W \Gamma_s}{Y_t + Y_L}[\bar{\varrho}_e(k_0)]^2 \exp(-jk_0L). \tag{4.72}$$

The voltage V_R also causes generation of a wave to the right, with potential $\phi_{s2}(\omega)$, say, at port 2. This is given by equation (4.52), with V_R replacing V_t. Using equation (4.70) for V_R, we have

$$\phi_{s2}(\omega) = -\frac{\omega W \Gamma_s}{Y_t + Y_L} \phi_{i1}(\omega)|\bar{\varrho}_e(k_0)|^2 \exp(-jk_0L), \tag{4.73}$$

where we have used the relation $\bar{\varrho}_e(-k_0) = \bar{\varrho}_e^*(k_0)$, since $\varrho_e(x)$ is real. The total potential of the wave to the right, denoted by $\phi_{t2}(\omega)$ at port 2, also includes a contribution due to the incident wave, given by $\phi_{i1}(\omega) \exp(-jk_0L)$. The total is divided by the incident wave potential $\phi_{i1}(\omega)$ to give the transmission coefficient $t_{12}(\omega)$. It is convenient to introduce $G_a(\omega)$ by using equation (4.60), giving

$$t_{12}(\omega) \equiv \frac{\phi_{t2}(\omega)}{\phi_{i1}(\omega)} = \left[1 - \frac{G_a(\omega)}{Y_t + Y_L}\right] \exp(-jk_0L). \tag{4.74}$$

The power ratios for reflection and transmission of waves incident on port 1 are, from equations (4.72) and (4.74),

$$|r_1(\omega)|^2 = \frac{G_a^2}{|Y_t + Y_L|^2} \tag{4.75}$$

and

$$|t_{12}(\omega)|^2 = 1 - \frac{G_a^2 + 2G_aG_L}{|Y_t + Y_L|^2}, \tag{4.76}$$

where G_L is the real part of the load admittance Y_L. There is also some power delivered to the load, given by $P_L = \frac{1}{2}|V_R|^2 G_L$. The power of the incident surface wave is, from equation (4.51), $P_s = \frac{1}{4}\omega W|\phi_{i1}|^2/\Gamma_s$. The ratio of these powers is the power conversion coefficient, $C_1(\omega)$. Using equation (4.70), we have

$$C_1(\omega) \equiv \frac{P_L}{P_s} = \frac{2G_aG_L}{|Y_t + Y_L|^2}. \tag{4.77}$$

The sum of the three power coefficients, equations (4.75), (4.76) and (4.77), is unity, so that all the power incident on the transducer is accounted for. The power conversion coefficient, equation (4.77), also applies for a launching transducer driven by a source with internal admittance Y_L, giving the ratio of surface wave power generated (in one direction) divided by the available electric power. This can be shown by simple network analysis, and is of course expected by reciprocity. Some useful deductions from the above equations are:

(a) If the transducer is shorted, so that $Y_L = \infty$, the reflection and conversion coefficients are both zero, and the transmission coefficient is unity.

(b) If a loss-less reactance is connected across the terminals, cancelling the transducer susceptance, then $Y_t + Y_L = G_a$. The reflection coefficient is then unity, and no power is converted or transmitted. This applies for any frequency. The reactance required will normally be inductive.

(c) If the transducer is electrically matched, $Y_L = Y_t^*$ so that $Y_t + Y_L = 2G_a$. In this case the power reflection and transmission coefficients are both $\frac{1}{4}$, and the conversion coefficient is $\frac{1}{2}$.

Equations (4.75) and (4.77) also show that there is a simple relationship between

the power reflection and conversion coefficients:

$$|r_1(\omega)|^2 = \frac{G_a}{2G_L} C_1(\omega). \tag{4.78}$$

The scattering coefficients derived above are consistent with experimental results, and with theoretical results obtained from the crossed-field network model, for uniform transducers operated at the fundamental centre frequency [84, 85]. In particular, the prediction of a zero reflection coefficient for a shorted transducer agrees well with experiment, though not for a single-electrode transducer on a strongly piezoelectric substrate (such as lithium niobate) — in this case electrode interactions are strong, and the quasi-static approximation is not valid.

Scattering matrix. The above equations may be combined to give a more general relationship between the potentials of incident and transmitted surface waves at the two ports and the transducer voltage and current. This situation is shown in Figure 4.8. The potentials of incident waves are denoted by ϕ_i, and those of waves leaving the transducer by ϕ_t, with additional subscripts 1 or 2 to indicate that these potentials are evaluated at port 1 or port 2, respectively. The four surface waves are all taken to be beams of width W, aligned with the active region of the transducer. The voltage across the bus-bars is V, and the transducer draws a current I.

The scattering matrix S_{ij} is defined by the equation

$$\begin{bmatrix} \phi_{t1} \\ \phi_{t2} \\ I/(\omega W) \end{bmatrix} = \begin{bmatrix} 0 & S_{12} & S_{13} \\ S_{21} & 0 & S_{23} \\ S_{31} & S_{32} & S_{33} \end{bmatrix} \begin{bmatrix} \phi_{i1} \\ \phi_{i2} \\ V\Gamma_s \end{bmatrix}, \tag{4.79}$$

where the coefficients

$$\begin{aligned} \cdot &= \\ \cdot &= - \qquad\qquad), \\ \cdot &= - \qquad\qquad), \\ \cdot &= \end{aligned}$$

where $Y_t(\omega)$ is the transducer admittance, given by equation (4.55).

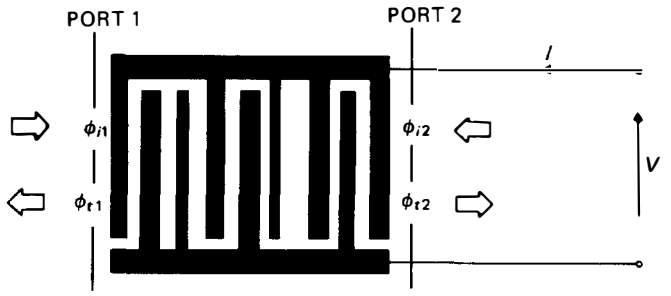

FIGURE 4.8. Parameters used in scattering matrix.

4.5. TRANSDUCERS WITH REGULAR ELECTRODES

In Section 4.4 the various properties of an unapodised transducer were derived, using the quasi-static approximation, and the results were expressed in terms of the electrostatic charge density $\varrho_e(x)$ and its Fourier transform $\bar{\varrho}_e(\beta)$. In general, these functions can only be evaluated numerically, and some methods were discussed in Section 4.3.2 above. However, for an important class of transducer structures the electrostatic charge density can be obtained analytically, and hence analytic results can be obtained for the transducer properties. This approach yields an element factor for transducer analysis, so that the analysis becomes very similar to the delta-function model of Section 4.1 above.

4.5.1. Electrostatic Charge Density and Element Factor

We consider the transducer shown in Figure 4.9(a). The electrodes here are assumed to be *regular*, that is, they all have the same width, a, and the centre-to-centre spacing, p, is constant throughout the array. Within the transducer, the fraction of the area covered by the electrodes is a/p, and this is called the *metallisation ratio*.

For unit voltage applied across the bus-bars, the electrostatic charge density $\varrho_e(x)$ is obtained by charge superposition. As in Section 4.4, equation (4.54), we have

$$\varrho_e(x) = \sum_{n=1}^{N} \hat{P}_n \varrho_{en}(x), \tag{4.80}$$

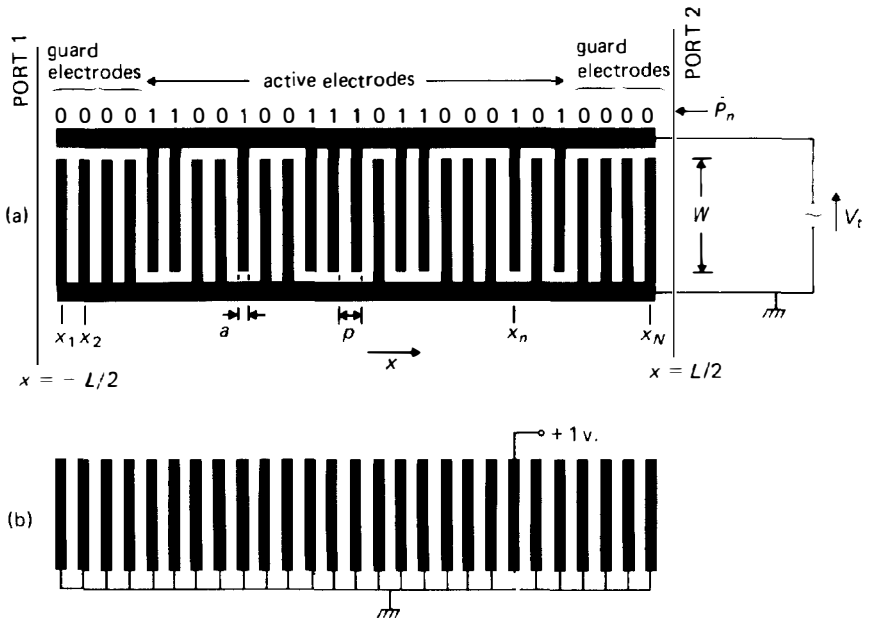

FIGURE 4.9. Transducer with regular electrodes.

where $\hat{P}_n = 1$ or 0 is the polarity of electrode n, as shown in Figure 4.9(a). The function $\varrho_{en}(x)$ is defined as the electrostatic charge density produced on the electrodes when unit voltage is applied to electrode n, with all the other electrodes grounded. This situation is illustrated in Figure 4.9(b). Now, the charge density produced here is largely determined by the geometry of electrode n and of a few neighbouring electrodes on either side. Here the electrodes all have the same geometry. It follows that, provided electrode n is not near either end of the array, the function $\varrho_{en}(x)$ is much the same for all electrodes, though it will of course have a lateral displacement corresponding to the electrode position [104, 105].

To exploit this feature, we define a more basic function $\varrho_f(x)$. We consider an infinite array of regular electrodes, as shown in Figure 4.10. One electode is centred at the origin $x = 0$ and has unit voltage applied, while all the other electrodes are grounded. The electrostatic charge density for this case is defined to be $\varrho_f(x)$, and will be called the *elemental charge density*.

For the finite array of Figure 4.9, electrode n is taken to be centred at $x = x_n$, and it follows that

$$\varrho_{en}(x) \approx \varrho_f(x - x_n) \tag{4.81}$$

provided electrode n is not near either end of the array. For the electrodes near the ends this relation is not valid. However, the contributions that the electrodes make to the total charge density $\varrho_e(x)$ depend also on the polarities $\hat{P}_n$, as shown by equation (4.80). It is assumed here that $\hat{P}_n = 0$ for the electrodes near the ends, as in Figure 4.9, so that the functions $\varrho_{en}(x)$ for these electrodes will not contribute to $\varrho_e(x)$. We thus have

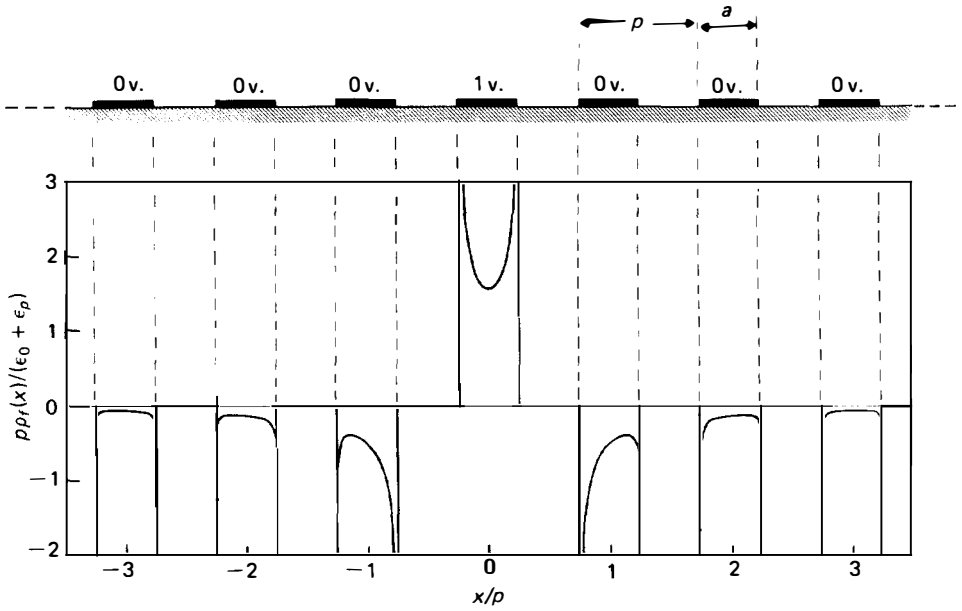

FIGURE 4.10. Elemental charge density $\varrho_f(x)$, for $a/p = \frac{1}{2}$.

$$\varrho_e(x) \approx \sum_{n=1}^{N} \hat{P}_n \varrho_f(x - x_n). \tag{4.82}$$

The electrodes at the two ends, with $\hat{P}_n = 0$, are described as *guard electrodes*, and are introduced in order to minimise end effects [104, 105]. Equation (4.82) becomes exact if an infinite number of guard electrodes is used at each end. However, the equation is found to be a good approximation if only a few are used, and for most practical purposes six guard electrodes at each end are sufficient. In the following analysis it is assumed that the number of guard electrodes is sufficient to make equation (4.82) valid to the required degree of accuracy. The electrodes in between the two groups of guard electrodes are called "active electrodes".

Equation (4.82) may be used to express the transducer response in terms of an element factor and an array factor. We first define an array factor in the x-domain by the relation

$$A_f(x) = \sum_{n=1}^{N} \hat{P}_n \delta(x - x_n) \tag{4.83}$$

so that equation (4.82) can be written

$$\varrho_e(x) = \int_{-\infty}^{\infty} A_f(x') \varrho_f(x - x') \mathrm{d}x' = A_f(x) * \varrho_f(x), \tag{4.84}$$

where the asterisk indicates convolution. In the β-domain, the Fourier transform $\bar{\varrho}_e(\beta)$ of $\varrho_e(x)$ is obtained by using the convolution theorem; $A_f(x)$ and $\varrho_f(x)$ are transformed to give $\bar{A}_f(\beta)$ and $\bar{\varrho}_f(\beta)$ respectively, and $\bar{\varrho}_e(\beta)$ is then given by the product

$$\bar{\varrho}_e(\beta) = \bar{A}_f(\beta)\bar{\varrho}_f(\beta), \tag{4.85}$$

where, from equation (4.83) the array factor $\bar{A}_f(\beta)$ is give by

$$\bar{A}_f(\beta) = \sum_{n=1}^{N} \hat{P}_n \exp(-j\beta x_n). \tag{4.86}$$

As shown in Section 4.4, nearly all the transducer properties are directly related to $\bar{\varrho}_e(\beta)$, the exception being the capacitance C_t which is considered below. For example, when a voltage V_t is applied, the potential $\phi_{s1}(\omega)$ of the surface wave emerging at port 1 is given by equation (4.50), and with the aid of equation (4.85) this becomes

$$\phi_{s1}(\omega) = j\Gamma_s V_t \bar{A}_f(k_0)\, \bar{\varrho}_f(k_0) \exp(-\tfrac{1}{2} j k_0 L). \tag{4.87}$$

Here the function $\bar{A}_f(k_0)$ is an array factor, while the elemental charge density $\bar{\varrho}_f(k_0)$ has the role of an element factor. Thus the response is expressed in a simple form, similar to the delta-function model of Section 4.1. For most transducers it is found that the array factor varies with frequency much more rapidly than the elemental charge density $\bar{\varrho}_f(k_0)$, so that the array factor alone gives a good approximation to the shape of the frequency response.

An analytic solution for the elemental charge density has been given by Peach [97] and by Datta and Hunsinger [106]. A derivation is given in Appendix C, making use of the electrostatic analysis in Section 3.1. The function $\varrho_f(x)$, giving the charge density in the x-domain, is given by equation (C.20), and is shown in Figure 4.10 for

a metallisation ratio $a/p = \frac{1}{2}$. It should be noted that the charge density is quantitatively significant only for the electrode centred at $x = 0$ and for a few electrodes on either side, though it is infinite at the edges of each electrode.

For most calculations the transformed function $\bar{\varrho}_f(\beta)$ is required, and Appendix C shows that this is given by

$$\bar{\varrho}_f(\beta) = (\varepsilon_0 + \varepsilon_p^T) \frac{2 \sin \pi s}{P_{-s}(-\cos \Delta)} P_m(\cos \Delta), \quad \text{for } m \leqslant \frac{\beta p}{2\pi} \leqslant m + 1, \quad (4.88)$$

where

$$\Delta = \pi a/p$$

$$s = \beta p/(2\pi) - m$$

$P_{-s}(-\cos \Delta)$ is a Legendre function

$P_m(\cos \Delta)$ is a Legendre polynomial.

This equation gives $\bar{\varrho}_f(\beta)$ for all β; the integer m must be chosen according to the value of β, and the parameter s is always in the range $0 \leqslant s \leqslant 1$. Appendix C gives some properties of Legendre functions. Since $\varrho_f(x)$ is clearly real and even, it follows from Fourier analysis that $\bar{\varrho}_f(\beta)$ is also real and even, so that $\bar{\varrho}_f(-\beta) = \bar{\varrho}_f(\beta)$. The variable β occurs only in the normalised form of the product βp. The function is shown in Figure 4.11, for several values of the metallisation ratio a/p. It consists of a sequence of lobes, all with the same shape, with relative amplitudes determined by the

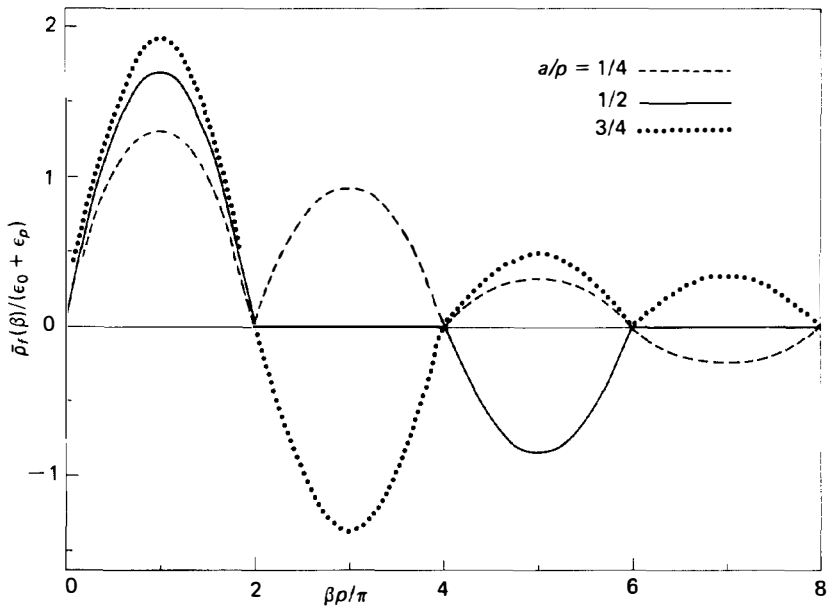

FIGURE 4.11. Elemental charge density, in the β-domain.

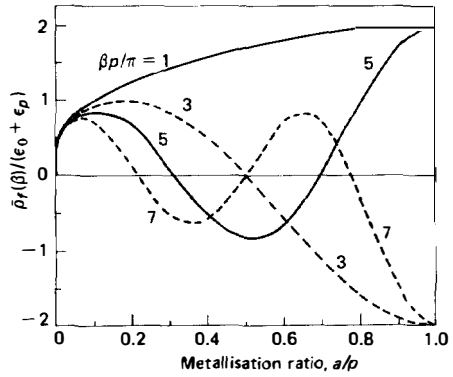

FIGURE 4.12. Elemental charge density: values at the peaks of the lobes, as functions of metallisation ratio.

polynomials $P_m(\cos \Delta)$ in equation (4.88). The relative amplitudes of the lobes are strongly influenced by the ratio a/p. This is clarified by Figure 4.12, where the values of $\bar{\varrho}_f(\beta)$ at the peaks of the lobes are plotted against a/p. The peaks of the lobes occur at $\beta = \pi/p$ and odd multiples of this value.

For a uniform single-electrode transducer, the peaks of the lobes occur at the fundamental centre frequency ω_c and at the odd harmonics, and the curves shown in Figure 4.12 give directly the relative harmonic strengths, as first pointed out by Engan [107].

The transducer capacitance C_t may be found by summing the electrostatic charges on all the electrodes connected to one bus-bar, as shown by equation (4.57). For transducers with regular electrodes, it is convenient to evaluate the net electrostatic charges on the electrodes when the charge density is $\varrho_f(x)$. These are denoted by Q_m, where $m = 0$ for the electrode at $x = 0$, $m = \pm 1$ for the electrodes on either side, and so on. Thus

$$Q_m = \int_{mp-a/2}^{mp+a/2} \varrho_f(x)\,\mathrm{d}x, \tag{4.89}$$

which gives the charge per unit width in the y-direction. When unit voltage is applied across a transducer, the charge on electrode n due to the voltage on electrode m is $W\hat{P}_m Q_{m-n}$. The total charge on electrode n is denoted q_n, and is thus given by

$$q_n = W \sum_{m=1}^{N} \hat{P}_m Q_{m-n}. \tag{4.90}$$

The total electrostatic charge on all the electrodes connected to the upper bus is equal to the capacitance C_t, and is given by

$$C_t = \sum_{n=1}^{N} \hat{P}_n q_n. \tag{4.91}$$

The capacitance is therefore readily found from the net charges Q_m, defined by equation (4.89). The charges are functions of the metallisation ratio a/p, and are given by equation (C.27) of Appendix C. In the particular case of $a/p = \frac{1}{2}$, the charges

are given by the simple formula

$$Q_m = \frac{4(\varepsilon_0 + \varepsilon_p^T)}{\pi(1 - 4m^2)}, \quad \text{for } a/p = \tfrac{1}{2}. \tag{4.92}$$

4.5.2. End Effects

In practice, interdigital transducers often do not have the guard electrodes shown in Figure 4.9, and consequently the charge densities on the electrodes at and near the ends are distorted. These distortions are known as *end effects*. They affect the frequency response of the transducer, though the perturbation is small if the transducer has many electrodes. For example, in a transducer with more than, say, twenty electrodes, end effects generally have little effect on the frequency response, and are significant only if a very accurate response is required.

To analyse end effects, it is necessary to solve for the electrostatic charge distribution numerically, using methods discussed in Section 4.3.2 above [98, 108]. In addition, some of the tabulated results for withdrawal-weighted transducers [90, 100] give information on end effects. The effects cannot be characterised straightforwardly; they depend on the frequency and on the electrode structure. To give a quantitative example, in a uniform single-electrode transducer operated at the centre frequency ω_c of the fundamental pass-band, the coupling due to the electrode at the end is reduced by 29%, while that due to the adjacent electrode is increased by 5% [98].

The charge superposition principle can be used to simplify the analysis a little if the functions $\varrho_{en}(x)$ are first calculated numerically [104]. As mentioned in Section 4.5.1, most of the $\varrho_{en}(x)$ can be approximated by displaced versions of $\varrho_f(x)$; numerical calculations are needed only for the electrodes near the ends. The total electrostatic charge density on the transducer can then be obtained by using equation (4.80), and this is valid for any sequence of electrode polarities. Some examples showing net electrode charges corresponding to the functions $\varrho_{en}(x)$ are given in Ref. [104].

4.5.3. Transducer Response in Terms of Gap Elements

The above analysis gives the transducer response in terms of an array of elements, each associated with one electrode. An alternative formulation gives the response in terms of elements associated with the inter-electrode gaps [104, 109]. From equation (4.85), the electrostatic charge density, in the β-domain, is $\bar{\varrho}_e(\beta) = \bar{A}_f(\beta)\bar{\varrho}_f(\beta)$, with the array factor given by

$$\bar{A}_f(\beta) = \sum_{n=1}^{N} \hat{P}_n \exp(-j\beta x_n) = \sum_{n=1}^{N-1} \hat{P}_{n+1} \exp[-j\beta(x_n + p)]. \tag{4.93}$$

Here the second form follows because $x_{n+1} = x_n + p$ and $\hat{P}_1 = 0$. If the second form is multiplied by $\exp(j\beta p)$ and then subtracted from the first form, it is found that $\bar{A}_f(\beta)$ can be written as a sum of terms involving $(\hat{P}_{n+1} - \hat{P}_n)$. This enables the charge density $\bar{\varrho}_e(\beta)$ to be written as

$$\bar{\varrho}_e(\beta) \approx \bar{A}_g(\beta)\bar{\varrho}_g(\beta), \tag{4.94}$$

where the new array factor is

$$\bar{A}_g(\beta) = \sum_{n=1}^{N-1} (\hat{P}_{n+1} - \hat{P}_n) \exp[-j\beta(x_n + p/2)], \tag{4.95}$$

and the new elemental charge density is

$$\bar{\varrho}_g(\beta) = -\tfrac{1}{2}j\bar{\varrho}_f(\beta)/\sin(\beta p/2). \tag{4.96}$$

Here $\bar{\varrho}_f(\beta)$ is given by equation (4.88), and the term $\sin(\pi s)$ is cancelled by the term $\sin(\beta p/2)$ above. In consequence, $\bar{\varrho}_g(\beta)$ varies less rapidly with β than $\bar{\varrho}_f(\beta)$. In the x-domain, the inverse transform $\varrho_g(x)$ can be shown to be the charge density on an infinite array of regular electrodes, when those to the right of the origin have unit voltage and those to the left are grounded [109]. The new array factor, equation (4.95), corresponds to an array of elements located at $x = x_n + p/2$, the centres of the inter-electrode gaps, the strength of each element being zero if the adjacent electrodes have the same polarity; if the polarities are different, the strength is ± 1.

This formulation is often convenient for transducer analysis. It also corresponds to the delta-function analysis of Section 4.1, giving a formal justification for the delta-function approach. The element factor E in Section 4.1 can now be identified as

$$E = (\omega\Gamma_s)^{1/2}\bar{\varrho}_g(k_0). \tag{4.97}$$

4.6. ADMITTANCE OF UNIFORM TRANSDUCERS

A uniform transducer is defined here as an unapodised transducer with regular electrodes, in which the electrode polarities $\hat{P}_n$ have a repetitive pattern instead of the arbitrary choice assumed in Section 4.5. Nearly all surface-wave devices have at least one uniform transducer, and the repetitive nature enables some simple and useful expressions for the main properties to be obtained. In this section the capacitance and the acoustic conductance and susceptance are considered, though other properties, such as the conversion coefficient, are readily obtained from the analysis given here.

The commonest types of uniform transducer are shown in Figure 4.13. Defining S_e as the number of electrodes per period, the types with $S_e = 2$ or 4 are the conventional "single-electrode" or "double-electrode" transducers, respectively, and a type with $S_e = 3$ is also shown. Engan [83] has derived the transducer properties from equations describing multi-strip couplers. The method used here is applicable for any repetitive polarity sequence, with any value of S_e. The presence of guard electrodes is assumed, so that end effects can be ignored. However, as discussed in Section 4.5, the analysis gives a good approximation if there are no guards (as in Figure 4.4, for example), provided the number of periods is not too small.

4.6.1. Acoustic Conductance and Susceptance

From Section 4.5, equation (4.83), the array factor can be written

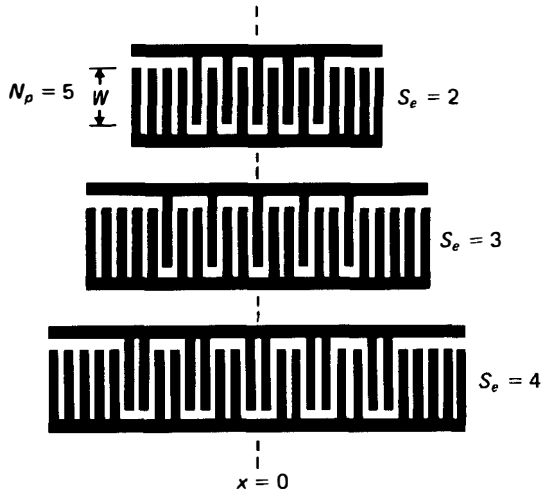

FIGURE 4.13. Uniform transducers, with guard electrodes.

$$A_f(x) = \sum_{n=1}^{N} \hat{P}_n \delta(x - x_n). \tag{4.98}$$

For uniform transducers, this can be expressed as the convolution

$$A_f(x) = A_N(x) * A_1(x), \tag{4.99}$$

where $A_1(x)$ is an array factor for one period of the transducer, and $A_N(x)$ is a sequence of delta functions with spacing equal to the transducer period, pS_e. For convenience these are defined such that $A_f(x)$ is symmetrical, so that $\bar{\varrho}_e(k_0)$ will be real. From Figure 4.13, $A_1(x)$ is given by

$$\begin{aligned} A_1(x) &= \delta(x) && \text{for } S_e = 2 \text{ or } 3 \\ &= \delta(x + p/2) + \delta(x - p/2), && \text{for } S_e = 4. \end{aligned} \tag{4.100}$$

Defining N_p as the number of periods in the transducer, the factor $A_N(x)$ is

$$A_N(x) = \sum_{n=1}^{N_p} \delta[x - (2n - N_p - 1)pS_e/2]. \tag{4.101}$$

This factor has the same form for all uniform transducers. Its Fourier transform $\bar{A}_N(\beta)$ is a geometric progression which is readily summed to give

$$\bar{A}_N(k_0) = \frac{\sin(N_p k_0 pS_e/2)}{\sin(k_0 pS_e/2)}. \tag{4.102}$$

From equation (4.100), the transform of $A_1(x)$ gives

$$\begin{aligned} \bar{A}_1(k_0) &= 1, && \text{for } S_e = 2 \text{ or } 3 \\ &= 2\cos(k_0 p/2), && \text{for } S_e = 4 \end{aligned} \tag{4.103}$$

The transform of $A_f(x)$ is, from equation (4.99),

$$\bar{A}_f(k_0) = \bar{A}_N(k_0)\,\bar{A}_1(k_0). \tag{4.104}$$

This enables the parallel conductance to be calculated, since from equations (4.60) and (4.85),

$$G_a(\omega) = \omega W \Gamma_s |\bar{A}_f(k_0)\,\bar{\varrho}_f(k_0)|^2, \tag{4.105}$$

where $\bar{\varrho}_f(\beta)$ is the elemental charge density [equation (4.88)], W is the transducer aperture, and $k_0 = \omega/v_0$ is the free-surface wavenumber at frequency ω.

For a single-electrode transducer ($S_e = 2$) we have $\bar{A}_f(k_0) = \bar{A}_N(k_0)$, given by equation (4.102). This function has maxima with magnitude N_p at $k_0 = 2\pi M/(pS_e)$, where $M = 0, 1, 2, \ldots$. The frequencies of the maxima are $\omega = M\omega_c$, where $\omega_c = \pi v_0/p$ is the centre frequency of the fundamental response. The function is similar to Figure 4.2, but here the even harmonics are present as well as the odd ones. The harmonic strengths are strongly affected by the $\bar{\varrho}_f(k_0)$ term in equation (4.105). The even-numbered harmonics are eliminated because $\bar{\varrho}_f(k_0)$ is zero at these points, and in addition the $\bar{\varrho}_f(k_0)$ term suppresses the 3rd, 7th, 11th, . . . harmonics when $a/p = \frac{1}{2}$, as can be seen from Figure 4.11.

Similar remarks apply for the transducers with $S_e = 3$ and 4. In each case the fundamental response is centred at $\omega_c = 2\pi v_0/(pS_e)$. Harmonic responses are centred at frequencies $M\omega_c$, but are absent when M is a multiple of S_e because $\bar{\varrho}_f(k_0)$ is zero at these points. Thus for $S_e = 3$ the responses occur for $M = 1, 2, 4, 5, 7, \ldots$. For $S_e = 4$, the harmonics with $M = 2, 6, 10, \ldots$ are eliminated by the array factor for one period, equation (4.103), so for this case the responses occur only for odd values of M. In addition, harmonics in the region $2\pi < k_0 p < 4\pi$ disappear when $a/p = \frac{1}{2}$. For $S_e = 3$, this applies to the 4th and 5th harmonics, and for $S_e = 4$ it applies to the 5th and 7th harmonics.

If the number of periods, N_p, is not too small, a useful approximation can be obtained for the conductance in the region near the fundamental frequency ω_c. We define

$$X = N_p(\tfrac{1}{2}k_0 p S_e - \pi) = \pi N_p(\omega - \omega_c)/\omega_c, \tag{4.106}$$

which is proportional to the fractional deviation of ω from ω_c. When ω is close to ω_c, the array factor of equation (4.102) is approximately

$$\bar{A}_N(k_0) \approx -N_p \frac{\sin X}{X}(-1)^{N_p}. \tag{4.107}$$

If N_p is large, this function varies rapidly with ω. The conductance, equation (4.105), includes other frequency-dependent terms — the ω and $\bar{\varrho}_f(k_0)$ terms and, for $S_e = 4$, the array factor of equation (4.103) — but these vary slowly with ω. Thus, for frequencies

near ω_c the conductance may be approximated by

$$G_a(\omega) \approx G_a(\omega_c)\left[\frac{\sin X}{X}\right]^2. \tag{4.108}$$

The constant $G_a(\omega_c)$ depends on the value of S_e, and is given below.

An approximate form for the acoustic susceptance $B_a(\omega)$ may be obtained from equation (4.108). As shown in Section 4.4.2, the susceptance is the Hilbert transform of the conductance. With X given by equations (4.106), the required Hilbert transform is

$$\left[\frac{\sin X}{X}\right]^2 * \frac{-1}{\pi\omega} = \frac{\sin(2X) - 2X}{2X^2}. \tag{4.109}$$

This may be demonstrated by transforming to the time domain, multiplying by the transform of $(-1/\pi\omega)$, and then transforming back to the frequency domain. The relationships needed are given in Appendix A. Thus, for frequencies near ω_c the susceptance is given by

$$B_a(\omega) \approx G_a(\omega_c)\frac{\sin(2X) - 2X}{2X^2}. \tag{4.110}$$

The approximate expressions for $G_a(\omega)$ and $B_a(\omega)$, equations (4.108) and (4.110), are plotted in Figure 4.14. The total susceptance of the transducer is $\omega C_t + B_a(\omega)$, and the capacitive term ωC_t is often much larger than $G_a(\omega_c)$; in addition $B_a(\omega)$ is zero at the centre frequency ω_c. Thus, in many cases the acoustic susceptance $B_a(\omega)$ is of little practical consequence.

Experimental measurements of $G_a(\omega)$ and $B_a(\omega)$ generally agree well with

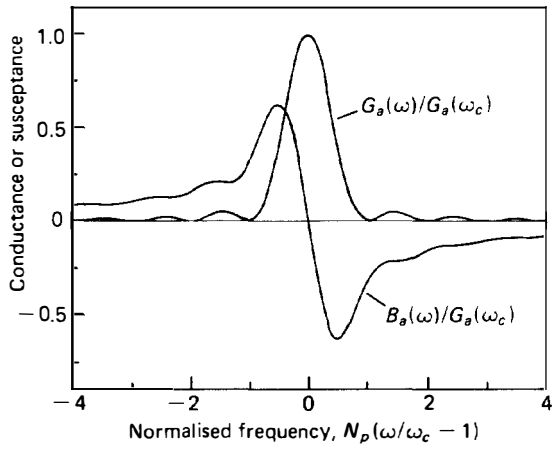

FIGURE 4.14. Acoustic conductance and susceptance for uniform transducers.

equations (4.108) and (4.110), as shown for example by Smith *et al.* [84] and Engan [83]. Usually there are also contributions due to bulk wave excitation, excluded in the above analysis, but provided N_p is not too small these are mostly confined to frequencies where the surface-wave terms are small. However, considerable distortion occurs if electrode interactions are strong.

For $M \leqslant S_e$, the conductance at the fundamental centre frequency ω_c and at the harmonics $M\omega_c$ can be written as

$$G_a(M\omega_c) = \alpha M \omega_c N_p^2 W \Gamma_s \left[\frac{2(\varepsilon_0 \quad \varepsilon_p^T) \quad (\pi s)}{} \right]^2, \tag{4.111}$$

where $\alpha = 1$ for $S_e = 2$ or 3. For $S_e = 4$, $\alpha = 2$ if $M = 1$ or 3 and $\alpha = 0$ if $M = 2$. Also, $s = M/S_e$ and $\Delta = \pi a/p$. Equation (4.111) follows from equation (4.105), with the array factor given by equations (4.102)–(4.104) and the elemental charge density $\bar{\varrho}_f(k_0)$ given by equation (4.88).

4.6.2. Capacitance

As shown by equation (4.91), the static capacitance of the transducer is

$$C_t = \sum_{n=1}^{N} \hat{P}_n q_n, \tag{4.112}$$

where N is the number of electrodes and q_n is the net electrostatic charge on electrode n when unit voltage is applied across the transducer. For a uniform transducer the electrode charges q_n in each period of the transducer are similar to those in other periods, and so the capacitance C_t is approximately proportional to the number of periods, N_p. This is not exactly true because the electrode charges are somewhat different near the ends of the transducer. For convenience an approximate formula is given here, assuming N_p to be large; the charges q_n are evaluated for each period assuming the transducer to be infinitely long, and C_t is then found by summing over N_p periods. Thus

$$C_t \approx N_p \sum_{n=1}^{S_e} \hat{P}_n q_n, \tag{4.113}$$

where $\hat{P}_n$ and q_n are evaluated for one period of a transducer of infinite length. The charges q_n are given by

$$q_n = W \sum_{r=-\infty}^{\infty} \sum_{i=1}^{S_e} \hat{P}_i Q_{i+rS_e-n}, \tag{4.114}$$

where Q_m is the charge on electrode n associated with the voltage on electrode $(n - m)$, as defined in equation (4.89). The summation over r in equation (4.114) may be done with the aid of equation (C.30) of Appendix C, and the remaining summations required are straightforward. For the transducers under consideration here, the result is

$$C_t = \gamma W N_p(\varepsilon_0 + \varepsilon_p^T) \frac{\sin(\pi/S_e)}{P_v(-\cos\Delta)} P_v(\cos\Delta), \tag{4.115}$$

where $\gamma = 1$, $4/3$ or 2 for $S_e = 2$, 3 or 4, respectively, and $v = -1/S_e$.

4.6.3. Comparative Performance

In comparing the behaviour of the transducers, an important quantity is the electrical Q-factor, here denoted by Q_t. At frequency ω_c and at the multiples of this frequency, the acoustic susceptance $B_a(\omega)$ is zero. We define Q_t as the ratio of the susceptance to the conductance at these frequencies, so that

$$Q_t = M\omega_c C_t / G_a(M\omega_c). \tag{4.116}$$

The value of Q_t will in general depend on the harmonic number, M. The reciprocal of Q_t is a measure of the surface-wave coupling strength, taking account of the transducer geometry and the parameters of the substrate material. It will be shown in Chapter 7 that this parameter has a strong influence on the bandwidth obtainable when the transducer is tuned in order to minimise its conversion loss.

The basic properties of the three types of transducer are summarised in Figure 4.15 and Table 4.1. For convenience, a normalised capacitance $\tilde{C}_t$, conductance $\tilde{G}_{aM}$ and Q-factor $\tilde{Q}_t$ are introduced, defined such that

$$C_t = W N_p(\varepsilon_0 + \varepsilon_p^T)\tilde{C}_t, \tag{4.117}$$

$$G_a(M\omega_c) = M\omega_c(\varepsilon_0 + \varepsilon_p^T)^2 N_p^2 W \Gamma_s \tilde{G}_{aM}, \tag{4.118}$$

$$Q_t = \tilde{Q}_t / [N_p(\varepsilon_0 + \varepsilon_p^T)\Gamma_s], \tag{4.119}$$

where C_t, $G_a(M\omega_c)$ and Q_t are given by equations (4.115), (4.111) and (4.116) above. The normalised parameters are independent of the substrate properties ε_p^T and Γ_s, and of the number of periods N_p and the aperture W. The capacitance and Q-factor are

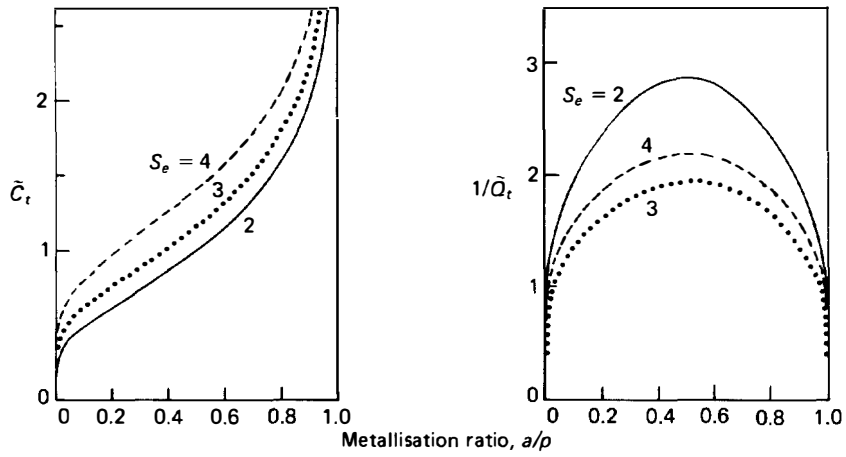

FIGURE 4.15. Uniform transducers: normalised capacitance and Q-factor, as functions of metallisation ratio.

TABLE 4.1
Data for uniform transducers, $a/p = \frac{1}{2}$

S_e	Normalised capacitance $\tilde{C}_t$	Harmonic number M	Normalised conductance $\tilde{G}_{aM}$	Normalised inverse Q-factor $1/\tilde{Q}_t$
2	1	1	2.871	2.871
3	1.155	1	2.231	1.932
		2	2.231	1.932
4	1.414	1	3.111	2.200
		2	0	0
		3	3.111	2.200

shown in Figure 4.15, plotted as functions of the metallisation ratio a/p. It can be seen that the metallisation ratio is not a critical parameter, and that for all three transducers the coupling strength is maximised for $a/p = \frac{1}{2}$. Numerical data are given in Table 4.1, for $a/p = \frac{1}{2}$. The coupling strength is strongest for the single-electrode transducer ($S_e = 2$). For $S_e = 3$ or 4, there is a harmonic with coupling strength equal to that of the fundamental. The capacitance is smallest for $S_e = 2$. Engan [83] has confirmed experimentally the values of $\tilde{C}_t$ and $\tilde{G}_{aM}$ in this table.

4.7. TWO-TRANSDUCER DEVICES

This section considers the analysis of a device comprising two interdigital transducers, each transducer having two terminals. One transducer is taken to be energised by a source with zero impedance, while the other is shorted. It is assumed that the transducers do not reflect incident surface waves in this situation, so that the quasi-static results of Section 4.4 can be used. It is also assumed that waves due to reflections from the edges of the substrate can be ignored, as is usually ensured by the use of acoustic absorbers. Reflections do however arise when the transducers are connected to finite electrical impedances, and this will be considered in Section 4.8. The analysis here is not valid if the transducers are of the unidirectional type using multi-strip couplers, described in Section 5.4, since these give appreciable reflections when they are shorted. Apodised transducers are introduced in this section, because the results of interest are meaningful only when a combination of transducers is considered.

Initially, a generalised transducer geometry is considered. For apodised transducers the more specialised case of regular electrodes is also considered, using the results of Section 4.5. This enables the response to be expressed in terms of an array factor and an element factor, as in the delta-function analysis of Section 4.1.

It is assumed that the transducer separation is sufficient to make electrostatic coupling between the transducers negligible, so that the current produced by the output transducer is entirely due to the surface waves incident on it.

4.7.1. Devices Using Unapodised Transducers

To analyse devices, it is convenient to define the frequency response, $H_t(\omega)$, of an unapodised transducer by the expression

$$H_t(\omega) = (\omega W \Gamma_s)^{1/2} \bar{\varrho}_e(k_0) \exp(-\tfrac{1}{2} j k_0 L). \tag{4.120}$$

The processes of launching and reception of surface waves can be written in terms of this function. For a launching transducer, with a voltage V_t applied, the surface wave potential at port 1 is, from equation (4.50),

$$\phi_{s1}(\omega) = jV_t H_t(\omega) \left[\frac{\Gamma_s}{\omega W}\right]^{1/2}. \tag{4.121}$$

For a receiving transducer, if the incident surface wave has a potential $\phi_{s1}(\omega)$ at port 1, the output current produced when the transducer is shorted is given by

$$I_{sc} = -j\phi_{i1}(\omega) H_t(\omega)(\omega W/\Gamma_s)^{1/2} \tag{4.122}$$

from equation (4.68).

These equations can be applied to the two-transducer device shown in Figure 4.16. For transducers A and B, the electrostatic charge density, for unit voltage applied across the bus-bars, is denoted by $\varrho_e^a(x)$ and $\varrho_e^b(x)$, respectively. Each of these functions is to be determined assuming the other transducer to be absent. To preserve the symmetry, different x-axes must be used for the two transducers; in each case the x-axis is directed away from the other transducer, and its origin is midway between the two acoustic ports. For each transducer, port 1 is defined as the port closest to the other transducer. The lengths of transducers A and B are respectively L_a and L_b. The frequency responses are $H_t^a(\omega)$ and $H_t^b(\omega)$, given by equation (4.120) with $\bar{\varrho}_e(k_0)$ given the superscript a or b and L given the corresponding subscript.

As shown in Figure 4.16, transducer A is connected to a source with zero impedance and voltage V_t, while transducer B is shorted. It is assumed that neither transducer reflects incident waves under these conditions, and that diffraction and attenuation are negligible. The wave incident on transducer B is therefore $\phi_{i1}(\omega) = \phi_{s1}(\omega) \exp(-jk_0 d)$, where d is the transducer separation. The ratio I_{sc}/V_t can then be found from equations (4.121) and (4.122). This ratio is denoted by $H_{sc}(\omega)$, and is given

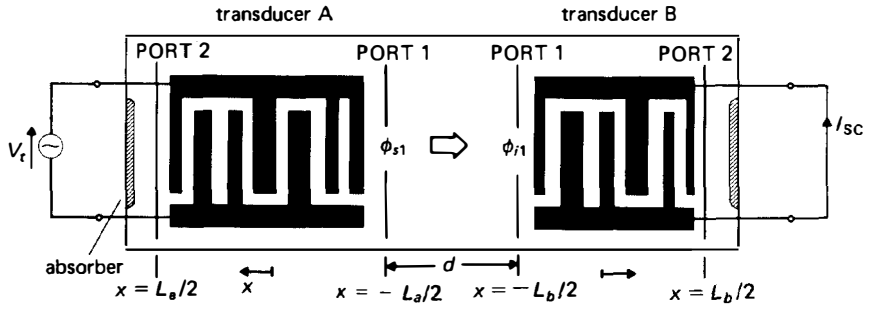

FIGURE 4.16. Two-transducer device, with unapodised transducers.

by

$$H_{sc}(\omega) \equiv I_{sc}/V_i = H_t^a(\omega)H_t^b(\omega) \exp(-jk_0 d). \quad (4.123)$$

This is called the *short-circuit response* of the device, since both transducers are connected to zero impedances.

Comparing equations (4.120) and (4.60) shows that the parallel conductance of an unapodised transducer is directly related to its frequency response:

$$G_a(\omega) = |H_t(\omega)|^2. \quad (4.124)$$

Thus, if the conductances of the two transducers are known, the magnitude of the device short-circuit response can be obtained directly.

4.7.2. Device Using One Apodised Transducer

We now consider the short-circuit response of the device in the upper part of Figure 4.17, where one transducer is apodised. The apodised transducer is assumed to have "dummy" electrodes in the acoustically inactive regions, so that the electrodes extend from both bus-bars and the breaks between them are small. This feature is commonly used in practice because the electrodes perturb the surface wave velocity; the addition of dummy electrodes gives a more uniform perturbation, and substantially reduces the consequent phase distortion of the surface wave [110].

Following Tancrell and Holland [79], the device is analysed by imagining it to be divided into a number of parallel "channels", whose edges correspond to the locations of the electrode breaks in the apodised transducer. Since diffraction is neglected, the launching and reception of surface waves in individual channels can be analysed independently. Thus, in each channel the electrodes of the apodised transducer constitute an imaginary unapodised transducer, and the apodised transducer may be replaced by an array of unapodised transducers, as in the lower part of Figure 4.17. The imaginary unapodised transducers, which can be analysed by methods given above, are electrically connected in parallel. Since the electrode resistivity is assumed to be negligible, the admittance of the apodised transducer is simply the sum of the admittances of the imaginary unapodised transducers. This approach is valid even if electrode interactions or bulk wave excitation are present, though the analysis here excludes these effects.

Consider first the response of transducer B, which is taken to be an unapodised transducer receiving surface waves and is assumed to be shorted. In channel j, the wave incident on port 1 is denoted $\phi_{i1}^j(\omega)$, and the width of channel j is denoted W_j. Considering the electrodes in this channel as a separate transducer, the output current produced when the transducer is shorted is I_{sc}^j, say, given by

$$I_{sc}^j = -j\omega W_j \phi_{i1}^j(\omega)\, \bar{\varrho}_e^b(k_0) \exp(-\tfrac{1}{2} jk_0 L_b) \quad (4.125)$$

from equation (4.68). The function $\bar{\varrho}_e^b(k_0)$ is the same in all channels because the transducer is unapodised. The total current I_{sc} is simply the sum of the I_{sc}^j. Using the frequency response defined in equation (4.120), this is

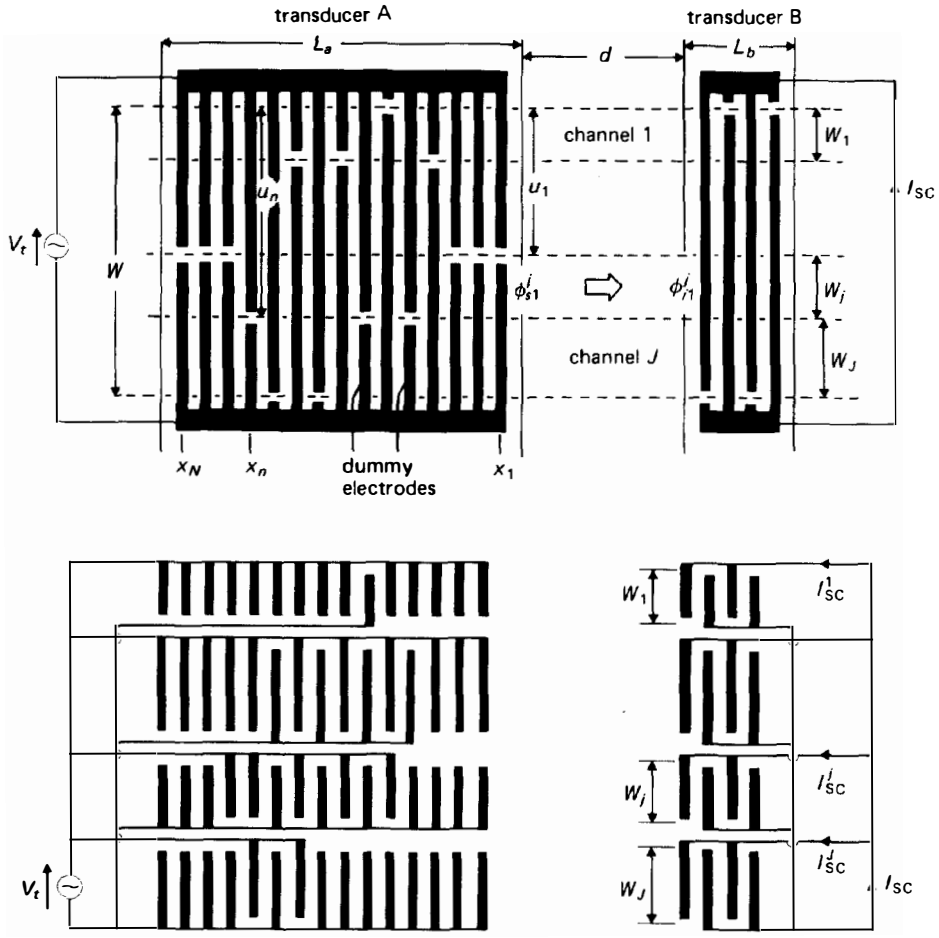

FIGURE 4.17. *Upper*: Two-transducer device with one transducer apodised. *Lower*: Equivalent representation as a network of unapodised transducers.

$$I_{sc} = -jH_t^b(\omega)(\omega W/\Gamma_s)^{1/2}\left[\sum_j W_j\phi^j_{i1}(\omega)/W\right]. \tag{4.126}$$

Here the term in square brackets is the average surface wave potential at the transducer input; the current is therefore the same as for a uniform input beam (equation 4.122), except that the average surface-wave potential is used.

For the apodised transducer, transducer A, we define $\varrho^a_{ej}(x)$ as the electrostatic charge density on the electrodes in channel j, when unit voltage is applied across the transducer, with Fourier transform $\bar{\varrho}^a_{ej}(\beta)$. Using this function, the potential of the wave generated in channel j, denoted by $\phi^j_{s1}(\omega)$, is given by equation (4.50). In addition, since there are no reflected waves, and diffraction and attenuation are

ignored, we have $\phi'_{i1}(\omega) = \phi'_{s1}(\omega) \exp(-jk_0 d)$. The output current is then given by equation (4.126), and is thus related to the input voltage V_t. We define the response $H_t^a(\omega)$ of transducer A such that the device short-circuit response is essentially the product of the transducer responses:

$$H_{sc}(\omega) \equiv I_{sc}/V_t = H_t^a(\omega) H_t^b(\omega) \exp(-jk_0 d) \tag{4.127}$$

as in the unapodised case. To satisfy this, the required definition for $H_t^a(\omega)$ is

$$H_t^a(\omega) = (\omega W \Gamma_s)^{1/2} \exp(-\tfrac{1}{2} jk_0 L_a) \sum_j W_j \bar{\varrho}_{oj}^a(k_0)/W. \tag{4.128}$$

For an unapodised transducer, this reduces to the form already given in equation (4.120). The definition can also be expressed in terms of the surface wave potentials at port 1 when a voltage V_t is applied across the transducer; equation (4.121) is thus valid for an apodised transducer if $\phi_{s1}(\omega)$ is replaced by the average of the $\phi'_{s1}(\omega)$. For an apodised transducer receiving a uniform surface-wave beam, the short-circuit current is found to be given by equation (4.122).

The response defined in equation (4.128) is valid only if at least one of the two transducers is unapodised, with its active region intercepting all of the surface waves generated (in one direction) by the other transudcer. It should also be noted that the simple relationship between $G_a(\omega)$ and $H_t(\omega)$ for an unapodised transducer, equation (4.124), is not valid for an apodised transducer.

4.7.3. Apodised Transducer with Regular Electrodes

If the electrodes are regular, so that they have the same width a and constant pitch p, the frequency response of an apodised transducer can be expressed in a convenient form, using the elemental charge distribution described in Section 4.5. As shown in Figure 4.17, it is assumed here that guard electrodes are included at both ends, thus minimising end effects.

The response is readily obtained from the definition of equation (4.128) and the analysis of Section 4.5.1, so the results are quoted here without the derivation. We define a parameter u_n as the location of the break between the electrodes centred at $x = x_n$, relative to the upper boundary of the active region, as in Figure 4.17. The transducer response is then given by

$$H_t(\omega) = (\omega W \Gamma_s)^{1/2} \bar{A}_f(k_0) \bar{\varrho}_f(k_0) \exp(-\tfrac{1}{2} jk_0 L), \tag{4.129}$$

where $\bar{\varrho}_f(k_0)$ is the elemental charge density defined in equation (4.88) and $\bar{A}_f(k_0)$ is an array factor defined by

$$\bar{A}_f(k_0) = \sum_{n=1}^{N} (u_n/W) \exp(-jk_0 x_n). \tag{4.130}$$

Thus the array factor is directly related to the transducer geometry. The formula can be applied to an unapodised transducer, in which case $\bar{A}_f(k_0)$ becomes the same as the definition given previously, equation (4.86).

An alternative formula can be given in terms of gap elements, using the equations

of Section 4.5.3. The result is

$$H_t(\omega) = (\omega W \Gamma_s)^{1/2} \bar{A}_g(k_0)\, \bar{\varrho}_g(k_0) \exp(-\tfrac{1}{2} j k_0 L), \tag{4.131}$$

where the elemental charge density $\bar{\varrho}_g(k_0)$ is given by equation (4.96) and the array factor $\bar{A}_g(k_0)$ is defined by

$$\bar{A}_g(k_0) = \sum_{n=1}^{N-1} \frac{u_{n+1} - u_n}{W} \exp[-jk_0(x_n + p/2)]. \tag{4.132}$$

This shows that, in x-domain, the array factor can be taken as a set of delta functions located at the centres of the inter-electrode gaps, with the strength of each delta function proportional to the distance over which the adjacent electrodes with different polarities overlap. The transducer can therefore be regarded as an array of elements associated with the gaps, as in the delta-function analysis of Section 4.1. The elements can be taken to be located in the regions where the polarities of adjacent electrodes are different, as in Figure 4.3. The analysis of Section 4.1 is thus justified, with the element factor E given by equation (4.97).

Transverse End Effect. In the above analysis it has been assumed that the charge density on each electrode is uniform across the width of each channel. There is however some distortion of the charge density in the region near the break, where the electrodes connected to the two bus-bars almost meet. To find the charge density in this region, a two-dimensional analysis is needed. Some results obtained by Wagers [111] show that the distortion extends a distance approximately equal to the width of the break.

For practical purposes, this "transverse end effect" can be allowed for by adjusting the source strengths. Thus, if the response is expressed in terms of gap elements, a small constant is added to the terms $(u_{n+1} - u_n)$ in equation (4.132). The value of the constant depends on the width of the break.

4.8. DEVICE RESPONSE ALLOWING FOR TERMINATING CIRCUITS

Up to this point, we have only considered the response of a two-transducer device for the case where the transducers are connected to zero electrical impedances. In this section the electrical impedances are allowed to be finite, as they must be in any practical situation. This analysis is needed to evaluate the insertion loss of a device and to assess the circuit effect, that is, the distortion of the device frequency response due to the use of finite impedances. In addition the analysis gives the triple-transit spurious signal, discussed in Section 4.2 above.

It is quite common to connect each transducer to the electrical source or load via a simple lumped-element circuit, in order to improve the electrical matching. The analysis here therefore allows for unspecified circuits. The circuits in the analysis may include stray components, such as the capacitance between the "live" bus and the package and the inductance of the transducer bond wires. They may also include some

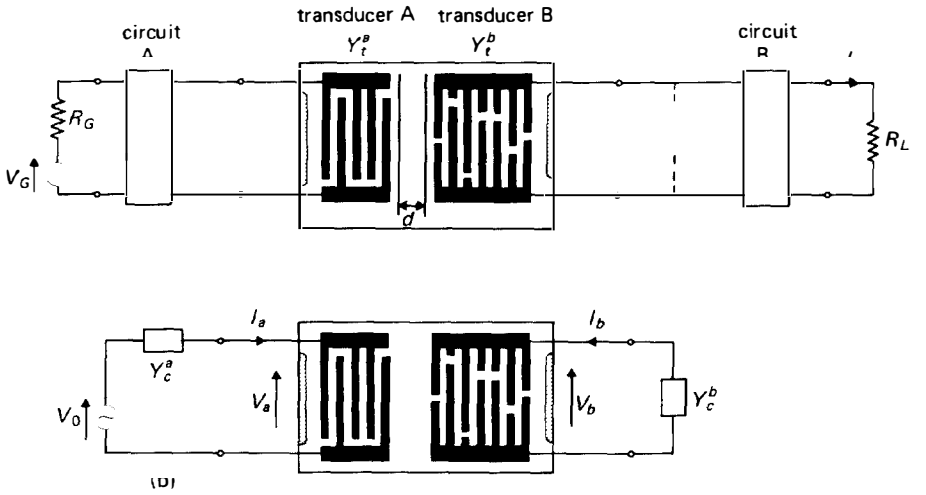

FIGURE 4.18. (a) Device analysis allowing for terminating circuits. (b) Equivalent circuit for analysis of multiple-transit terms.

resistance in order to model the resistivity of the transducer electrodes. Chapter 7 considers some specific circuits, and their effects on device performance.

It is assumed that the transducers do not reflect surface waves when they are shorted, as in previous sections. For finite terminating impedances the transducers reflect, and a triple-transit output signal is produced. The relative level of this signal is easily deduced if the transducers are unapodised. Consider the device shown in Figure 4.18(a), where the voltage on the output transducer, transducer B, is V_b. The main component of this voltage, denoted V_{b1}, is due to the wave generated by transducer A reaching transducer B directly. In addition there is a triple-transit component V_{b3}, due to reflection at transducer B and then again at transducer A, so that a second wave arrives at transducer B. The ratio of these components is therefore, for unapodised transducers,

$$V_{b3}/V_{b1} = r_1^a(\omega) r_1^b(\omega) \exp(-2jk_0 d), \tag{4.133}$$

where d is the distance between the adjacent transducer ports, and $r_1^a(\omega)$ and $r_1^b(\omega)$ are the reflection coefficients referred to these ports. The reflection coefficients are given by equation (4.72). The total voltage across transducer B is the sum of V_{b1} and V_{b3}, plus contributions due to additional transits; thus $V_b = V_{b1} + V_{b3} + V_{b5} + \ldots$.

In Figure 4.18(a), the load R_L develops a voltage V_L proportional to V_b. Thus V_L includes components proportional to V_{b1} and V_{b3}, with the ratio given by equation (4.133). If V_G is the open circuit of the generator, we define the ratio V_L/V_G to be the device frequency response $H(\omega)$. It follows that the response can be written as

$$H(\omega) \equiv V_L/V_G = H_1(\omega) + H_3(\omega) + H_5(\omega) + \ldots, \tag{4.134}$$

where $H_1(\omega)$ gives the main signal, due to the wave reaching transducer B directly, and

$H_3(\omega)$ gives the triple-transit signal. The ratio $H_3(\omega)/H_1(\omega)$ is equal to V_{b3}/V_{b1}, equation (4.133).

Equation (4.133) was derived assuming both transducers to be unapodised, and neglecting diffraction and attenuation. It will however be shown below that the response can be expressed as in equation (4.134), even when these assumptions are not valid. The results below involve the short-circuit response $H_{sc}(\omega)$. If the transducers are apodised, and diffraction and attenuation are significant, the analysis is still valid provided these factors are allowed for in the evaluation of $H_{sc}(\omega)$. However, the derivation of H_{sc} in Section 4.7 above assumes that diffraction and attenuation are negligible, and that at least one of the two transducers is unapodised.

Usually, the main response $H_1(\omega)$ in equation (4.134) is of most interest, the other terms being small unwanted components. It is therefore convenient to consider $H_1(\omega)$ first.

4.8.1. Main Response

The main response $H_1(\omega)$ is defined as the response obtained if reflections from the transducers are ignored. This is conveniently expressed by defining circuit factors $F_c^a(\omega)$ and $F_c^b(\omega)$. Considering circuit A and transducer A, at the input of the device in Figure 4.18(a), the circuit factor is defined as

$$F_c^a(\omega) = [V_a/V_G]_{V_b=0}, \tag{4.135}$$

where V_a and V_b are respectively the voltages across transducers A and B. The definition assumes that no acoustic waves are incident on the transducer, and it is therefore necessary to set $V_b = 0$ so that transducer B does not reflect. The circuit factor depends on the transducer admittance $Y_t^a(\omega)$ and the generator impedance R_G, as well as on the details of the circuit. For transducer B and circuit B, at the output, an imaginary current generator I_{sc} is connected between the terminals of the transducer and, with transducer A shorted so that it does not reflect, we define

$$F_c^b(\omega) = [I_L/I_{sc}]_{V_a=0}, \tag{4.136}$$

where I_L is the current in the load. The two definitions given by equations (4.135) and (4.136) are in fact equivalent, as can be shown using the reciprocity theorem of network analysis.

To find $H_1(\omega)$, the reflected surface waves are ignored. Thus V_a is given by equation (4.135) and I_L by equation (4.136), and we also have $I_{sc} = H_{sc}(\omega)\, V_a$, where $H_{sc}(\omega)$ is the short-circuit response. Thus

$$H_1(\omega) = V_L/V_G = H_{sc}(\omega)\, F_c^a(\omega) F_c^b(\omega) R_L, \tag{4.137}$$

which is essentially the product of the short-circuit response and the two circuit factors.

Since the multiple-transit terms $H_3(\omega)$, $H_5(\omega)$, . . . are usually small in comparison, the insertion loss of the device may be obtained approximately from $H_1(\omega)$. If P_G is the power available from the generator, and P_L the power delivered to the load, these are in the ratio

$$P_L/P_G = 4|H_1(\omega)|^2 R_G/R_L \tag{4.138}$$

and the insertion loss, in decibels, is

$$IL = -10 \log (P_L/P_G) \quad \text{(dB)}. \tag{4.139}$$

It is instructive to consider the theoretical minimum insertion loss predicted by these equations. Minimum loss is obtained if the circuits dissipate no power and the transducers are matched, so that all the power available from the generator is dissipated in transducer A, and all the power available from transducer B is dissipated in the load. These considerations determine the magnitudes of $F_c^a(\omega)$ and $F_c^b(\omega)$. For this calculation, diffraction and attenuation are assumed negligible and the short-circuit response $H_{sc}(\omega)$ of Section 4.7.2, equation (4.127), is used. Using standard network analysis, it is found that for this case the power ratio P_L/P_G is

$$[P_L/P_G]_{\max} = \tfrac{1}{4}|H_t^a(\omega)\, H_t^b(\omega)|^2/(G_a^a G_a^b), \tag{4.140}$$

where $H_t^a(\omega)$ and $H_t^b(\omega)$ are the transducer responses and G_a^a and G_a^b are their parallel conductances. Now, for an unapodised transducer we have, from equation (4.124), $G_a(\omega) = |H_t(\omega)|^2$. Thus, if both transducers are unapodised the maximum value of P_L/P_G is $\frac{1}{4}$, and hence the minimum insertion loss is 6 dB, as expected from the bidirectional nature of the transducers. If one of the transducers, say transducer B, is apodised, there is an additional contribution to the loss associated with the factor $|H_t^b(\omega)|^2/G_a^b$, which will be less than unity. This factor is sometimes known as the "apodisation loss".

In the above equations the multiple-transit terms have been excluded. The insertion loss including these terms is given by equation (4.138), with $H_1(\omega)$ replaced by the complete response $H(\omega)$, which is calculated below.

4.8.2. Multiple-transit Responses

To find the complete device response including the multiple-transit terms, it is convenient to consider the simpler circuit of Figure 4.18(b), which is equivalent to Figure 4.18(a). Here the generator and input circuit are replaced by a Thévenin equivalent, having a voltage generator V_0 in series with an admittance Y_c^a, where Y_c^a is the admittance "seen" by transducer A looking into the circuit in Figure 4.18(a). Using conventional network analysis, the equivalent generator voltage V_0 can be related to V_G using the circuit factor, giving

$$V_0/V_G = F_c^a(Y_t^a + Y_c^a)/Y_c^a. \tag{4.141}$$

At the output, transducer B is connected to an admittance Y_c^b, the admittance "seen" by transducer B looking into the circuit in Figure 4.18(a). The voltage on transducer B is denoted V_b, and this can be related to the load voltage V_L by means of the circuit factor:

$$V_L/V_b = -F_c^b R_L(Y_t^b + Y_c^b). \tag{4.142}$$

The device response $H(\omega)$ is defined as the ratio V_L/V_G, and in view of the above equations this can be obtained from the ratio V_b/V_0. For the main response, ignoring multiple transits, the ratio V_L/V_G is given by equation (4.137). The ratio of V_b/V_0 for the main response is denoted by $R_1(\omega)$, and can be obtained from equations (4.137), (4.141) and (4.142), giving

$$R_1(\omega) = \frac{-H_{sc} \cdot Y_c^a}{(Y_t^a + Y_c^a)(Y_t^b + Y_c^b)}. \tag{4.143}$$

To find the complete response, the behaviour of the surface wave device itself is expressed in terms of an admittance matrix [112]. We define V_a and V_b as the transducer voltages, and I_a and I_b as the transducer currents, as in Figure 4.18(b). For $V_b = 0$ is assumed that transducer B does not reflect surface waves, so that $I_a/V_a = Y_t^a$ and $I_b/V_a = H_{sc}(\omega)$. Similarly, for $V_a = 0$ we have $I_b/V_b = Y_t^b$ and, by reciprocity, $I_a/V_b = H_{sc}(\omega)$. The device therefore has an admittance matrix given by

$$\begin{bmatrix} I_a \\ I_b \end{bmatrix} = \begin{bmatrix} Y_t^a & H_{sc} \\ H_{sc} & Y_t^b \end{bmatrix} \cdot \begin{bmatrix} V_a \\ V_b \end{bmatrix}. \tag{4.144}$$

This enables the ratio V_b/V_0 to be evaluated. From Figure 4.18(b) we have $I_a = (V_0 - V_a)Y_c^a$ and $I_b = -Y_c^b V_b$. Using equation (4.144), and eliminating V_a, I_a and I_b, gives

$$V_b/V_0 = [R_1^{-1} + H_{sc}/Y_c^a]^{-1} \tag{4.145}$$

where R_1 is the function defined in equation (4.143). Using the binomial theorem, this is written as the series

$$V_b/V_0 = R_1[1 - R_1 H_{sc}/Y_c^a + (R_1 H_{sc}/Y_c^a)^2 + \ldots] \tag{4.146}$$

In this equation, the short-circuit response H_{sc} includes a factor giving the phase change due to the transducer separation. This can be seen, for example, in equation (4.127), where a term $\exp(-jk_0 d)$ is present. The function R_1, equation (4.143), is proportional to $H_{sc}(\omega)$, and therefore includes the same factor. Hence the first term of equation (4.146), which includes this factor, is the main response; the second term includes a factor with a phase change three times as large and is therefore the triple-transit term, and so on. The overall response of the device, $H(\omega)$, is defined as the ratio V_L/V_G, and can be obtained from equations (4.146), (4.141) and (4.142). However, since the contribution due to the main response, $H_1(\omega)$, has already been given in equation (4.137), it is sufficient to consider the ratios of the terms here. From equation (4.146), the ratio of the triple-transit response to the main response is

$$\begin{aligned} H_3(\omega)/H_1(\omega) &= -R_1 H_{sc}/Y_c^a \\ &= \frac{H_{sc}^2}{(Y_t^a + Y_c^a)(Y_t^b + Y_c^b)}, \end{aligned} \tag{4.147}$$

where equation (4.143) has been used for R_1. The corresponding ratios for additional transits of the device are readily obtained from equation (4.146) and the overall response $H(\omega)$ can be obtained by summing these terms, as in equation (4.134).

It is emphasised here that the result of equation (4.147) is valid if both transducers are apodised, and if diffraction and attenuation are significant, provided these factors are allowed for in evaluating $H_{sc}(\omega)$. The main assumption is that reflections are absent when the transducers are connected to zero impedances; this is required in

order to establish the admittance matrix of equation (4.144). In the particular case of unapodised transducers, with negligible diffraction and propagation loss, the triple-transit term can be expressed in terms of the transducer reflection coefficients, as shown by equation (4.133). This can be shown to be consistent with equation (4.147) by using the transducer reflection coefficient given in equation (4.72), together with the short-circuit response given by equations (4.123) and (4.120). However, for an apodised transducer a reflection coefficient cannot be defined straightforwardly because the amplitude of the reflected wave will vary across the aperture. Thus a more general approach, as given above, is called for.